

1  
2  
3  
4  
5  
6  
7  
8  
9  
10  
11  
12  
13  
14  
15  
16  
17  
18  
19  
20  
21  
22

**The dual function monoclonal antibodies VIR-7831 and VIR-7832 demonstrate potent in vitro and in vivo activity against SARS-CoV-2**

Andrea L. Cathcart<sup>1</sup>, Colin Havenar-Daughton<sup>1</sup>, Florian A. Lempp<sup>1</sup>, Daphne Ma<sup>1</sup>, Michael A. Schmid<sup>2</sup>,  
Maria L. Agostini<sup>1</sup>, Barbara Guarino<sup>2</sup>, Julia Di iulio<sup>1</sup>, Laura E. Rosen<sup>1</sup>, Heather Tucker<sup>1</sup>, Joshua Dillen<sup>1</sup>,  
Sambhavi Subramanian<sup>1</sup>, Barbara Sloan<sup>1</sup>, Siro Bianchi<sup>2</sup>, Dora Pinto<sup>2</sup>, Christian Saliba<sup>2</sup>, Katja Culap<sup>2</sup>,  
Jason A Wojcechowskyj<sup>1</sup>, Julia Noack<sup>1</sup>, Jiayi Zhou<sup>1</sup>, Hannah Kaiser<sup>1</sup>, Arthur Chase<sup>1</sup>, Martin Montiel-  
Ruiz<sup>1</sup>, Exequiel Dellota Jr.<sup>1</sup>, Arnold Park<sup>1</sup>, Roberto Spreafico<sup>1</sup>, Anna Sahakyan<sup>1</sup>, Elvin J. Lauron<sup>1</sup>, Nadine  
Czudnochowski<sup>1</sup>, Elisabetta Cameroni<sup>1</sup>, Sarah Ledoux<sup>1</sup>, Adam Werts<sup>3</sup>, Christophe Colas<sup>1</sup>, Leah Soriaga<sup>1</sup>,  
Amalio Telenti<sup>1</sup>, Lisa A. Purcell<sup>1</sup>, Seungmin Hwang<sup>1</sup>, Gyorgy Snell<sup>1</sup>, Herbert W. Virgin<sup>1</sup>, Davide Corti<sup>2</sup>,  
Christy M. Hebner<sup>1\*</sup>

<sup>1</sup>Vir Biotechnology, San Francisco, California 94158, USA

<sup>2</sup>Humabs Biomed SA, a subsidiary of Vir Biotechnology, 6500 Bellinzona, Switzerland

<sup>3</sup>Lovelace Biomedical, Albuquerque, New Mexico 87108, USA

\*corresponding author: [chebner@vir.bio](mailto:chebner@vir.bio)

23 **ABSTRACT**

24 **VIR-7831 (sotrovimab) and VIR-7832 are dual action monoclonal antibodies (mAbs) targeting the**  
25 **spike glycoprotein of severe acute respiratory syndrome coronavirus 2 (SARS-CoV-2). VIR-7831**  
26 **and VIR-7832 were derived from a parent antibody (S309) isolated from memory B cells of a 2003**  
27 **severe acute respiratory syndrome coronavirus (SARS-CoV) survivor. Both mAbs contain an “LS”**  
28 **mutation in the Fc region to prolong serum half-life. In addition, VIR-7832 encodes an Fc GAALIE**  
29 **mutation that has been shown previously to evoke CD8<sup>+</sup> T-cells in the context of an in vivo viral**  
30 **respiratory infection. VIR-7831 and VIR-7832 potently neutralize wild-type and variant authentic**  
31 **virus in vitro as well as variant pseudotyped viruses including the Omicron variant. In addition,**  
32 **they retain activity against monoclonal antibody resistance mutations conferring reduced**  
33 **susceptibility to currently authorized mAbs. The VIR-7831/VIR-7832 epitope continues to be highly**  
34 **conserved among circulating sequences consistent with the high barrier to resistance observed in**  
35 **vitro. Furthermore, both mAbs can recruit effector mechanisms in vitro that may contribute to**  
36 **clinical efficacy via elimination of infected host cells. In vitro studies with these mAbs demonstrated**  
37 **no enhancement of infection. In a Syrian Golden hamster proof-of concept wildtype SARS-CoV-2**  
38 **infection model, animals treated with VIR-7831 had less weight loss, and significantly decreased**  
39 **total viral load and infectious virus levels in the lung compared to a control mAb. Taken together,**  
40 **these data indicate that VIR-7831 and VIR-7832 are key agents in the fight against COVID-19.**

41

42 **INTRODUCTION**

43 The coronavirus disease (COVID-19) pandemic caused by severe acute respiratory syndrome coronavirus  
44 2 (SARS-CoV-2) has resulted in more than 260 million confirmed cases and over 5.2 million deaths  
45 worldwide<sup>1</sup>. SARS-CoV-2 infection results in a broad range of disease severity<sup>2</sup>. Infection fatality rates  
46 increase significantly with age, with 28.3% of COVID-19 patients over the age of 85 succumbing to

47 disease<sup>2</sup>. However, even in mild-to-moderate COVID-19 patients, significant post-infection sequelae can  
48 affect overall health and cause long-term disability<sup>3</sup>. While multiple SARS-CoV-2 vaccines are now  
49 available for use, issues of supply, vaccine hesitancy and emergence of variants may prevent rapid  
50 attainment of herd immunity<sup>4-9</sup>. In addition, there are individuals who remain at risk despite vaccination  
51 due to disease or underlying immunodeficiency. Thus, additional interventions and potential prophylactic  
52 agents are needed to reduce morbidity and mortality due to COVID-19.

53 Several monoclonal antibodies (mAbs) targeting the SARS-CoV-2 spike protein have recently been  
54 authorized or approved for use in early treatment of COVID-19 patients<sup>10-13</sup> and clinical data have shown  
55 promising results in treatment and prophylactic studies<sup>12-16</sup>. However, rapidly spreading variants exhibit  
56 reduced susceptibility in vitro to some currently authorized antibodies that target the receptor binding  
57 motif (RBM) of the viral spike (S) glycoprotein<sup>10,11,17,18</sup>. Therefore, mAbs targeting unique S epitopes are  
58 needed for use alone or in combination with current agents for the treatment and prevention of COVID-  
59 19. Furthermore, in addition to viral neutralization, antibodies possessing potent effector function to aid in  
60 the killing of virally infected cells and the elicitation of T cell immunity could significantly assist in  
61 halting disease progression<sup>19-21</sup>.

62 VIR-7831 and VIR-7832 are dual action mAbs derived from the parent antibody S309 identified from a  
63 2003 SARS-CoV survivor<sup>22</sup>. These mAbs target an epitope containing a glycan (at position N343) that is  
64 highly conserved within the Sarbecovirus subgenus in a region of the S receptor binding domain (RBD)  
65 that does not compete with angiotensin converting enzyme 2 (ACE2) binding<sup>23</sup>.<sup>10,11,17,18</sup> The variable  
66 region of VIR-7831 and VIR-7832 have been engineered for enhanced developability. In addition, both  
67 antibodies possess an Fc “LS” mutation that confers extended half-life by binding to the neonatal Fc  
68 receptor<sup>24-26</sup>. VIR-7832 is identical to VIR-7831 with the exception of the addition of a 3 amino acid  
69 GAALIE (G236A, A330L, I332E) modification to the Fc domain<sup>27</sup>. The GAALIE modification has  
70 previously been shown in vitro to enhance binding to FcγIIa and FcγIIIa receptors, decrease affinity for

71 FcγIIb compared to typical IgG1 and evoke protective CD8<sup>+</sup> T-cells in the context of viral respiratory  
72 infection in vivo<sup>28,29</sup>.

73 Here we characterize the antiviral activity of VIR-7831 and VIR-7832. These mAbs effectively neutralize  
74 SARS-CoV-2 live virus in vitro as well as in pseudotyped virus assays against emerging variants of  
75 concern and variants that confer resistance to currently authorized or approved mAbs<sup>30</sup>. In addition to the  
76 neutralizing capacity, both antibodies demonstrate potent effector function and mediate antibody  
77 dependent cellular cytotoxicity (ADCC) and antibody dependent cellular phagocytosis (ADCP) in vitro.  
78 Furthermore, resistance selection experiments and epitope conservation analyses indicate the potential for  
79 a high barrier to resistance. Data derived from the Syrian golden hamster model demonstrates efficacy in  
80 a proof-of-concept in vivo model. Taken together, these data indicate that VIR-7831 and VIR-7832 are  
81 promising key components of the arsenal in the fight against COVID-19.

## 82 **RESULTS**

### 83 **VIR-7831 and VIR-7832 bind SARS-CoV-2 spike and effectively neutralize live virus in vitro.**

84 Previously published work showed that S309 bound SARS-CoV-2 recombinant and cell surface-  
85 associated S and neutralized live virus in vitro<sup>22</sup>. We initiated these studies by repeating and extending  
86 these earlier results. To determine the binding activity of VIR-7831 and VIR-7832 to the SARS-CoV-2 S,  
87 enzyme-linked immunosorbent assay (ELISA), surface plasmon resonance (SPR) and flow cytometry  
88 assays were utilized. VIR-7831 and VIR-7832 bound to recombinant S RBD (amino acids 331-541) with  
89 EC<sub>50</sub> values of 20.40 ng/mL and 14.9 ng/mL, respectively, by ELISA (**Figure 1a**). Using SPR, both  
90 antibodies demonstrated potent binding to recombinant S RBD with an equilibrium constant (K<sub>d</sub>) of 0.21  
91 nM (**Figure 1b**). As antibody recognition of cell surface-bound S could mediate killing of virally infected  
92 cells, flow cytometry-based studies using cells transiently transfected with a S-encoding plasmid were  
93 used to examine antibody binding to cell surface-expressed S trimer. By this method, both VIR-7831 and  
94 VIR-7832 bound efficiently to surface-expressed S (**Figure 1c**).

95 To examine neutralization capacity, VIR-7831 and VIR-7832 were tested in a VeroE6 cell-based live  
96 SARS-CoV-2 virus system against the Washington 2019 (wild-type) virus as well as against the Alpha  
97 (B.1.1.7), Beta (B.1.351), Gamma (P.1), Delta (B.1.617.2) and Kappa (B.1.617.1) variants.  
98 Concentration-dependent viral neutralization of the Washington 2019 strain was observed for both  
99 antibodies, with geometric mean  $IC_{50/90}$  values of 100.1/186.3 ng/mL and 78.3/253.1 ng/mL, respectively  
100 (**Figure 1d**).  $IC_{50/90}$  values observed for VIR-7831 and VIR-7832 against the Beta, Gamma, Delta and  
101 Kappa variant viruses were similar to those against the wild-type strain. A slight shift in the VIR-  
102 7831/VIR-7832  $IC_{50/90}$  compared to wild-type was observed for the Alpha variant. VIR-7831 showed a 3-  
103 fold and 4.1-fold shift in  $IC_{50}$  and  $IC_{90}$ , respectively, against the Alpha variant compared to wild-type  
104 while VIR-7832 had a 3.1-fold shift in  $IC_{50}$  and 3.7-fold shift in  $IC_{90}$  versus wild-type (**Figure 1d, Table**  
105 **1**). As variant evolution is a natural part of SARS-CoV-2 biology and emerging live virus variants are not  
106 always readily accessible for testing, a vesicular stomatitis virus (VSV)-based pseudotyped virus system  
107 targeting Vero E6 cells was used to examine VIR-7831 and VIR-7832 neutralization against emergent  
108 variants (**Table 2**). Fold-changes in VIR-7831 and VIR-7832  $IC_{50}$  values compared to wild-type against  
109 pseudotyped virus expressing spike from the Alpha, Beta, Gamma, Delta or Kappa variants were similar  
110 to those observed in the authentic virus system. VIR-7831 was tested against an extended panel of  
111 pseudotyped viruses incorporating emerging variants as well as variants deemed as Variants of Concern  
112 (VOC) or Variants of Interest (VOI) by the World Health Organization (WHO). VIR-7831 retained  
113 activity in vitro against all variants tested with fold changes in  $IC_{50}$ s ranging from 0.4- to 2.3-fold (**Table**  
114 **2**).

115 **Neutralization of pseudotyped virus encoding Omicron substitutions.** On November 26, 2021, the  
116 WHO designated Omicron (B.1.1.529) as an official VOC. Omicron is reported to encode ~30  
117 substitutions in the spike, including substitutions that may render some currently authorized or approved  
118 COVID-19 mAbs inactive<sup>31-33</sup>. VIR-7831 was tested against a pseudotyped virus encoding the most  
119 frequent Omicron spike haplotype from the GISAID database as of December 2, 2021. This haplotype has

120 been found in multiple regions of the world including South Africa, Ghana, Botswana, United Kingdom,  
121 Netherlands, Portugal, Germany, Hong Kong, Australia and Austria. VIR-7831 retains activity against the  
122 Omicron pseudotyped virus with a fold change in IC<sub>50</sub> of 2.7 (Figure 2a and 2b). VIR-7831 was also  
123 tested against a panel of available pseudotyped viruses encoding a subset of individual mutations found in  
124 the Omicron spike (Figure 2a). These pseudotyped virus data demonstrate that VIR-7831 retains  
125 neutralizing activity against all tested individual Omicron substitutions including the G339D, S375F,  
126 K417N, N440K, S477N, T478K, E484A, Q493R and N501Y substitutions found in the RBD. The spike  
127 amino acids G339 and N440 are both part of the VIR-7831 epitope. In vitro studies using pseudotyped  
128 virus encoding either the G339D or N440K substitutions show that VIR-7831 retains activity against  
129 these spike substitutions (with IC<sub>50</sub> fold changes of 1.2 and 0.5, respectively) (Figure 2a, 2b). In addition,  
130 a lysine substitution has been detected at the VIR-7831 epitope position R346 in a small proportion of  
131 available Omicron sequences as of December 2, 2021 (16/334, 5.3% prevalence). VIR-7831 also retains  
132 activity in vitro against pseudotyped virus carrying the individual R346K substitution with a 0.7-fold-  
133 change in IC<sub>50</sub> (Figure 2a). These in vitro pseudotyped virus data indicate that VIR-7831 is expected to  
134 retain activity and potency against the Omicron variant of concern.

135 **VIR-7831 and VIR-7832 exhibit potent effector function in vitro.** Although direct antiviral  
136 mechanisms are crucial to provide protection, Fc-dependent mechanisms mediated by interaction with Fc  
137 gamma receptors (FcγRs) on immune cells or with complement, can contribute to overall potency in vivo.  
138 The potential for VIR-7831 and VIR-7832 to mediate effector functions were assessed in vitro by  
139 measuring binding to FcγRs and C1q and in assays designed to demonstrate antibody-dependent cellular  
140 cytotoxicity (ADCC) or antibody-dependent cellular phagocytosis (ADCP)<sup>34-37</sup>.

141 Antibody binding to the human activating FcγRIIa (low-affinity R131 and high affinity H131 alleles),  
142 FcγRIIIa (low-affinity F158 and high-affinity V158 alleles), and to the inhibitory FcγRIIb were examined  
143 using SPR (**Supplemental figure 1a**). VIR-7831 similarly bound both the H131 and R131 alleles of  
144 FcγRIIa and binds FcγRIIb. VIR-7831 bound both FcγRIIIa alleles, with reduced binding to the F158

145 allele compared to V158, as is characteristic for human IgG1<sup>38</sup>. Binding of VIR-7831 to C1q was similar  
146 to the parental antibody (S309-LS) (**Supplemental figure 1b**). As previously reported for antibodies  
147 encoding the GAALIE mutation<sup>27,39</sup>, VIR-7832 bound with comparatively higher affinity to activating  
148 FcγRIIa and FcγRIIIa than VIR-7831 (**Supplemental figure 1a**). Conversely, VIR-7832 showed reduced  
149 affinity for FcγIIb and abrogation of binding to C1q (**Supplemental figure 1b**).

150 The antibodies were also assessed for the ability to activate human FcγRIIa, FcγRIIb or FcγRIIIa, using a  
151 Jurkat cell reporter assay<sup>40</sup> (**Figure 3a-d**). S309-GRLR, which contains the effector function-abrogating  
152 G236R, L328R mutations was used as a negative control. Cells stably transfected with the SARS-CoV-2  
153 spike protein (CHO-CoV-2-Spike) served as target cells. Both VIR-7831 and the parental S309-LS  
154 activated signaling of the higher-affinity allele FcγRIIa (H131) but did so less efficiently than the  
155 GAALIE-containing antibody VIR-7832 (**Figure 3a**) while VIR-7831, VIR-7832 and S309-LS induced  
156 similar low-level activation of the inhibitory receptor FcγRIIb (**Figure 3b**). VIR-7831 demonstrated  
157 substantially lower activation of FcγRIIIa F158 versus V158 as expected while VIR-7832 showed  
158 increased activation of both alleles of FcγRIIIa (F158 and V158) (**Figures 3c,d**).

159 To further elucidate the effector function potential of the antibodies, ADCC and ADCP assays were  
160 performed using donor PBMCs or NK cells as effector cells and CHO cells stably expressing S (CHO-  
161 CoV-2-Spike) as target cells (**Figure 3e-g**). The ability of antibodies to activate NK cell-mediated killing  
162 was measured in vitro using two genotyped donors expressing homozygous low-affinity (F/F158) or high-  
163 affinity (V/V158) (**Figure 3e-f**). Compared to the parental mAb S309-LS, VIR-7831 had slightly  
164 increased capacity to induce NK cell-mediated ADCC when using cells from either F/F158 or V/V158  
165 donors. As expected, VIR-7832 induced NK cell-mediated ADCC in cells from donors expressing the  
166 low-affinity F/F158 allele of FcγRIIIa more efficiently than VIR-7831. These results were confirmed with  
167 NK cells from a heterozygous donor (F/V158).

168 The ability of VIR-7831 and VIR-7832 to facilitate ADCP by primary CD14<sup>+</sup> monocytes was measured in  
169 vitro by exposing freshly isolated human PBMCs to CHO-CoV-2-Spike cells that were pre-incubated

170 with antibody (**Figure 3g**). VIR-7831, VIR-7832 and S309-LS induced similar levels of ADCP by CD14<sup>+</sup>  
171 monocytes. These results indicate that VIR-7831 and VIR-7832 have the potential to trigger ADCC and  
172 ADCP of cells displaying SARS CoV-2 S protein.

173 **Subneutralizing levels of VIR-7831 and VIR-7832 do not enhance virus uptake, replication or**  
174 **cytokine production in vitro.** One potential concern with any antibody therapeutic targeting a viral agent  
175 is the possibility of antibody-dependent enhancement (ADE). ADE is an in vivo phenomenon in which  
176 the presence of an antibody worsens disease. There are several in vitro assays that may provide plausible  
177 correlates for ADE in vivo, though none of these have been proven relevant to COVID-19 as to date ADE  
178 has not been observed in trials of monoclonal antibodies or plasma<sup>13,15,41,42</sup>. ADE can occur by several  
179 potential mechanisms<sup>43</sup>. Poorly neutralizing antibodies or subneutralizing levels of antibody could  
180 theoretically facilitate enhanced virus entry and infection through Fc receptor interactions. A second  
181 theoretical mechanism involves antibody-antigen complex formation leading to enhanced cytokine  
182 production. A third mechanism of ADE has been observed in a porcine model of influenza where the  
183 kinetics of viral fusion to the target cell was enhanced in a Fab-dependent manner by fusion-enhancing  
184 non-neutralizing antibodies<sup>44,45</sup>.

185 To explore whether VIR-7831 and VIR-7832 exhibit in vitro activities that might be related to ADE in  
186 vivo, we evaluated SARS-CoV-2 replication in human cells that express FcγRs: monocyte-derived  
187 dendritic cells (moDCs), peripheral blood mononuclear cells (PBMCs) and the human U937 macrophage  
188 cell line (**Supplemental Figure 2a-b**). Subneutralizing concentrations of VIR-7831 and VIR-7832 were  
189 precomplexed with SARS-CoV-2 (MOI =0.01) and added to target cells. Using immunostaining methods,  
190 at 24 hours post-infection no productive entry of SARS-CoV-2 into moDCs, PBMCs, or U937 cells was  
191 observed in the presence or absence of either mAb, while VeroE6 control cells demonstrated  
192 internalization in all conditions evaluated. Reduced internalization of SARS-CoV-2 in VeroE6 cells was  
193 observed at the highest concentration of VIR-7831 and VIR-7832 (p-value <0.05), indicating effective  
194 virus neutralization prevented virus entry. Using a focus forming assay, virus replication and secretion of



195 infectious virus were detectable by 48 hours post-infection in VeroE6 cells, with comparable levels of  
196 replication in the presence or absence of VIR-7831 or VIR-7832. However, no replication of SARS-CoV-  
197 2 was detected in moDCs, PBMCs or U937 cells regardless of antibody treatment, indicating lack of  
198 productive SARS-CoV-2 infection of these cells, consistent with previously published data<sup>46</sup>.

199 To evaluate the potential for VIR-7831 and VIR-7832 to enhance cytokine release upon SARS-CoV-2  
200 infection in FcγR-expressing cells, cytokines and chemokines were measured in the supernatants from  
201 cells infected with SARS-CoV-2-in the presence of VIR-7831 or VIR-7832 (**Supplemental figure 2c**).  
202 Levels of IFN-γ, IL-10, IL-6, IL 8, IP-10, MCP-1, and TNF-α in the supernatant were quantified by MSD  
203 at 24- and 48-hours post-infection. For all cell types evaluated, cytokine/chemokine production was  
204 similar between all antibody concentrations tested and the no antibody control at both 24- and 48-hours  
205 post-infection. Taken together, these in vitro data indicate that neither VIR-7831 nor VIR-7832 exhibit in  
206 vitro activities that have been proposed to possibly correlate with ADE in vivo.

207 **VIR-7831 and VIR-7832 have a high barrier to resistance in vitro and do not display cross-**  
208 **resistance with other SARS-CoV-2 mAbs.** We next determined whether resistant variants could be  
209 elicited by serial passage of SARS-CoV-2 in the presence of VIR-7832. As VIR-7831 and VIR-7832  
210 differ only in the Fc region of the antibody, resistance selection experiments were conducted with VIR-  
211 7832 as a proxy for both antibodies. SARS-CoV-2 was subjected to 10 passages in the presence of VIR-  
212 7832 at fixed concentrations of ~10x, 20x, 50x or 100x IC<sub>50</sub> (1, 2, 5, or 10 μg/mL) in VeroE6 cells. No  
213 CPE was detected in wells passaged with antibody through 10 passages, while CPE was observed in the  
214 no antibody control in all passages. Similarly, no virus was detected by focus forming assay at any  
215 concentration of VIR-7832 through all 10 passages even at the lowest concentration tested.

216 As no viral breakthrough was observed in the fixed concentration resistance selection, a second method  
217 was employed wherein SARS-CoV-2 virus was passaged in sub-IC<sub>50</sub> concentrations of antibody followed  
218 by subsequent passaging in the presence of increasing concentrations of mAb in an attempt to force  
219 resistance emergence (**Supplemental Figure 3**). Passaging was performed in duplicate wells to account

220 for founder effects, and concentration increases for each well were based on CPE observations. Five  
221 sequential passages were conducted using increasing concentrations of VIR-7832 at 0.5, 1, 2, 5 and ~10x  
222  $IC_{50}$  (0.05, 0.1, 0.2, 0.5, 1  $\mu\text{g}/\text{mL}$ ; **Supplemental Figure 3a**), though no CPE was observed by passages 4  
223 and 5 (0.5 and 1  $\mu\text{g}/\text{mL}$ , respectively) indicating that variants originally selected at the lower  
224 concentrations were either unfit or susceptible to the higher concentrations of antibody. To further assess  
225 whether resistance mutations could be generated, selection was restarted using passage 3 virus generated  
226 with ~2x  $IC_{50}$  (0.2  $\mu\text{g}/\text{mL}$ ) of VIR-7832 in duplicate wells at ~2x and ~5x  $IC_{50}$  (0.2, 0.5  $\mu\text{g}/\text{mL}$ ),  
227 generating two passage lineages (**Supplemental Figure 3b-c**).

228 Supernatants were evaluated for detectable virus at each passage by focus forming assay and cell  
229 supernatants from viral passages containing detectable virus were tested in SARS-CoV-2 neutralization  
230 assays to evaluate  $IC_{50}$  shifts as a marker of reduced susceptibility (**Supplemental Table 1**). With the  
231 exception of passage 8, modest fold changes were observed, with shifts in  $IC_{50}$  values ranging from 5.4-  
232 to 6.5-fold compared to the wild-type SARS-CoV-2 stock virus. In lineage 1, the passage 8 virus  
233 displayed a >10-fold shift in  $IC_{50}$  (greater than highest concentration tested). Sequence analysis detected  
234 an identical 4 amino acid insertion in the N-terminal domain (215-216insKLRS) and 5 amino acid  
235 deletion in correspondence of the furin cleavage site (675-679del) in both lineages at all passages  
236 sequenced, as well as the amino acid substitution E340A in lineage 1, and R682W, and V1128F in  
237 lineage 2. The deletion at amino acids 675-679 has been previously described during passaging of SARS-  
238 CoV-2 in tissue culture suggesting enrichment to be a result of cell culture adaptation<sup>47</sup> while the 215-  
239 216insKLRS was detected in the input virus. Neither 215-216insKLRS nor R682W variants were highly  
240 enriched with passaging (**Supplemental Table 1**) and enrichment of 675-679del and V1128F did not  
241 profoundly alter the VIR-7832  $IC_{50}$ . However, appearance of the E340A variant at 98.7% did correlate  
242 with a >10-fold shift in  $IC_{50}$  suggesting this variant may confer resistance.

243 To evaluate whether amino acid variants identified in the resistance selection conferred reduced  
244 susceptibility to VIR-7831 and VIR-7832, neutralization of pseudotyped viruses encoding the S variants

245 was assessed (**Supplemental Table 2**). VIR-7831 and VIR-7832 neutralized R682W and V1128F SARS-  
246 CoV-2 pseudotyped virus spike variants with IC<sub>50</sub> values similar to wild type (< 2-fold change in IC<sub>50</sub>)  
247 indicating that these variants do not alter susceptibility. In contrast, E340A conferred reduced  
248 susceptibility to VIR-7831 and VIR-7832 (> 100-fold change in IC<sub>50</sub>) indicating that E340A is a VIR-  
249 7831/VIR-7832 monoclonal antibody resistance mutation (MARM).

250 As VIR-7831/VIR-7832 demonstrated a unique in vitro resistance profile, we investigated the potential  
251 for cross-resistance to MARMs that confer reduced susceptibility to the authorized monoclonal antibodies  
252 bamlanivimab, imdevimab and casirivimab<sup>10,11,48–50</sup> using pseudotyped virus. Notably, some of these  
253 mutations are found in highly prevalent variants of concern<sup>18,51,52</sup>. VIR-7831 effectively neutralized  
254 pseudotyped viruses expressing spike MARMs that alter bamlanivimab, casirivimab and/or imdevimab  
255 activity (**Table 3**). Fold changes in IC<sub>50</sub> values compared to wild-type were <3-fold for 18/19 variants  
256 tested. A modest 3.4-fold shift in the VIR-7831 IC<sub>50</sub> was observed for the V445A variant that confers  
257 reduced susceptibility to imdevimab. These data indicate that VIR-7831/VIR-7832 does not display cross-  
258 resistance with currently authorized mAbs and supports the potential combination use of VIR-7831/VIR-  
259 7832 with other mAb therapeutics.

260 **The VIR-7831/VIR-7832 epitope is highly conserved among SARS-CoV-2 sequences.** The parental  
261 antibody of VIR-7831 and VIR-7832 (S309) binds to a highly conserved sarbecovirus epitope that is  
262 potentially intolerant of variation. To investigate the current state of epitope conservation, >4,500,000  
263 spike sequences from SARS-CoV-2 deposited in the GISAID database as of November 11, 2021 were  
264 examined for epitope variation. More than 99.6% conservation is seen for those amino acids comprising  
265 the epitope among currently available sequences for all positions including 15/23 amino acid positions  
266 that were  $\geq 99.99$  conserved (**Table 4**).

267 VIR-7831 activity against viral mutants carrying single substitutions in the epitope was assessed in  
268 pseudotyped virus assays. VIR-7831 effectively neutralized epitope variants at most amino acid positions  
269 tested (**Supplemental Table 5**). A moderate shift in activity was observed for the K356T variant (5.9-fold

270 shift in IC<sub>50</sub>). Variants at two positions, E340 and P337, resulted in significant IC<sub>50</sub> shifts indicating  
271 reduced susceptibility to VIR-7831. Moderate shifts in potency were observed for P337H and P337T  
272 variants (5.13- and 10.62-fold, respective) while more significant shifts in potency were observed for  
273 P337L/R/K and E340A/K/G/Q (18.21-fold to >300-fold). Notably, these variants are detected in a low  
274 number of sequences and do not have a pattern that suggest emergence in the GISAID database (296 and  
275 223 variant counts out of >4,500,000 sequences for P337 and E340, respectively). This observation is  
276 consistent with the possibility that substitutions at these positions come with a fitness cost to the virus.

### 277 **VIR-7831 reduces weight loss, total viral load and infectious virus levels in a hamster model of**

278 **SARS-CoV-2 infection.** To evaluate the efficacy of VIR-7831 in vivo, the hamster model was utilized.

279 As it was unknown what effect the LS mutation would have in the hamster, a non-LS version of VIR-  
280 7831 (SGHmAb-no-LS) was used for these experiments. Hamsters were administered SGHmAb-no-LS  
281 intraperitoneally at Day -1 (30, 5, 0.5 or 0.05 mg/kg) or Day -2 (15, 5, 0.5 or 0.05 mg/kg) prior to  
282 intranasal SARS-CoV-2 inoculation (**Figure 4a**). Using body weight as a marker of degree of clinical  
283 disease, doses of  $\geq 5$ mg/kg resulted in significantly reduced weight loss at Day 4 compared to controls.  
284 (**Figure 4b-e**). Significant decreases in lung viral load were also observed at  $\geq 5$ mg/kg as measured by  
285 RT-qPCR (**Figures 4f-g**). Day 4 TCID<sub>50</sub> measurements indicated that antibody administered at  $\geq 0.5$   
286 mg/kg resulted in significantly lower levels of infectious virus in lung tissue compared to controls  
287 (**Figure 4h-i**). Notably, across these experiments, no enhancement of disease was observed in animals  
288 receiving SGHmAb-no-LS based on changes in weight, viral RNA in the lungs, or TCID<sub>50</sub> infectious  
289 virus levels. Collectively, these data indicate that VIR-7831 prevented in a dose-dependent fashion virus  
290 replication and morbidity in SARS-CoV-2 challenged hamsters without signs of ADE at any dose tested.

### 291 **DISCUSSION**

292 Here we show the in vitro and in vivo preclinical characterization of VIR-7831 and VIR-7832<sup>53-55</sup>. Both  
293 antibodies demonstrate high-affinity binding to S in vitro, including on the surface of cells, and  
294 effectively neutralize wildtype SARS-CoV-2 in a live virus assay. VIR-7831 and VIR-7832 retain activity

295 against the Alpha (B.1.1.7), Beta (B.1.351), Gamma (P.1), Delta (B.1.617.2) and Kappa (B.1.617.1)  
296 variants in an authentic virus system, consistent with data using pseudotyped viruses. Notably, VIR-7831  
297 retained activity in vitro against Omicron (B.1.1.529) pseudotyped virus encoding the currently most  
298 prevalent haplotype of Omicron spike. The activity data against the full combination of Omicron  
299 substitutions is consistent with single mutation neutralization data as well as previously published data  
300 examining the effects of RBD amino acid substitutions on VIR-7831 parental antibody (S309) binding  
301 using deep mutational scanning<sup>56</sup>. VIR-7831 also binds C1q, activate FcγRs and demonstrate ADCC and  
302 ADCP in vitro. Experiments in the hamster model of SARS-CoV-2 infection show proof-of-concept  
303 efficacy in vivo. Notably, in vitro and in vivo data did not provide any supporting evidence that these  
304 antibodies would demonstrate ADE in a clinical setting.

305 That VIR-7831 and VIR-7832 retain activity against spike variants in authentic virus and pseudotyped  
306 virus assays is a key finding at this stage of the pandemic. With the increased transmissibility and  
307 potential for more severe disease observed with these viruses, the availability of therapeutic or  
308 prophylactic mAbs that remains active against variants is essential. In addition to retaining activity  
309 against circulating WHO VOCs and VOIs, in pseudotyped virus experiments VIR-7831 showed no  
310 significant cross-resistance with variants that reduce the activity of other currently authorized or approved  
311 mAbs. These data additionally demonstrate the uniqueness of VIR-7831 and VIR-7832 and further  
312 highlight the utility VIR-7831 and VIR-7832 have, alone or in combination, as clinical agents.

313 Notably, even at this stage of the pandemic, the VIR-7831/VIR-7832 epitope remains highly conserved  
314 among available sequences of circulating virus with  $\geq 99.66\%$  conservation of epitope amino acids. This is  
315 consistent with the value of the strategy used for isolation of monoclonal antibodies that neutralize both  
316 SARS-CoV and SARS-CoV-2 based on the idea that these two virulent human viruses are  
317 phylogenetically divergent within the sarbecovirus subgenus. Furthermore, MARMs identified at  
318 positions P337 and E340 are present at very low levels among current sequences. That amino acids P337  
319 and E340 remain  $\geq 99.99\%$  conserved at this stage of the pandemic indicates that variants at these

320 positions may confer disadvantageous effects on the virus, consistent with the conservation of this epitope  
321 across the sarbecovirus family<sup>22</sup>.

322 Viral variants of concern for RBM-targeting mAbs are quickly spreading<sup>58</sup>. The vaccines presently being  
323 deployed around the world generate high-titer neutralizing antibodies that target the S protein RBM.  
324 Importantly, the RBM is highly immunodominant for responses to natural infection<sup>59</sup>. Vaccine-induced  
325 and convalescent immunity may therefore potentially put further mutational pressure on the RBM  
326 sequence to evade such antibody responses. In contrast, antibody responses overlapping with the VIR-  
327 7831/VIR-7832 epitope are limited after infection<sup>59</sup>, possibly because of the shielding effect of the highly  
328 conserved N343 glycan. In this regard the epitope may face less vaccine- or infection-generated immune  
329 pressure, potentially preserving this conserved epitope long-term.

330 Recent data have indicated that the cells used to generate live virus stocks and overexpression of  
331 ACE2/TMPRSS2 in target cells used for assays can affect mAb activity in vitro<sup>30,60</sup>. The VIR-7831/VIR-  
332 7832 parental antibody S309 seems particularly sensitive to in vitro methods using ACE2 overexpressing  
333 cells<sup>60</sup>. It is therefore notable that VIR-7831 displays significant efficacy in an in vivo proof-of-concept  
334 SARS-CoV-2 infection experiment using hamsters despite the fact that patterns of engagement of hamster  
335 FcRs by human IgG1 antibodies may not reflect patterns of human IgG1 antibodies with their cognate  
336 human FcRs. These findings argue that in vitro data derived from such ACE2 and/or TMPRSS2  
337 overexpression cell lines do not accurately reflect the in vivo antiviral capacity of tested mAbs.  
338 Furthermore, that the significant in vivo effects of VIR-7831 in the hamster model likely occurred in the  
339 absence of full effector functions due to species-specific interactions between antibodies and FcRs, argues  
340 that effects in COVID-19 patients incorporating both the neutralization capacity of the antibody plus the  
341 ability to harness the strength of the immune system could lead to positive clinical outcomes.

342 The clinical potential of VIR-7832, with the inclusion of the GAALIE Fc mutation, is of special interest  
343 in the context of SARS-CoV-2 infection. Previously published data by the Ravetch laboratory comparing  
344 the in vivo efficacy of a hemagglutinin-targeting mAb with and without inclusion of the GAALIE

345 mutation in a transgenic humanized Fc $\gamma$ R mouse model of influenza infection demonstrated superior  
346 efficacy of the GAALIE-containing antibody in both therapeutic and prophylactic experiments<sup>27</sup>. These  
347 effects were mediated by protective CD8<sup>+</sup> T cell responses elicited by the GAALIE antibody. Clinical  
348 data examining the contribution of the adaptive immune response in SARS-CoV-2 infection indicate that  
349 poor T cell induction correlates with severe disease (reviewed in <sup>61</sup>). Thus, the potential for VIR-7832 to  
350 augment the T cell response to SARS-CoV-2 infection could conceivably play a crucial role in limiting  
351 progression to severe COVID-19 disease or in treatment of severe established disease. This latter  
352 possibility is supported by recent publications showing that monoclonal antibodies with effector functions  
353 are especially effective in the therapeutic setting via recruitment of tissue-protective monocyte functions  
354 <sup>20</sup>, and that potency of antibodies in the pre-clinical mouse model does not correlate with in vitro  
355 neutralizing activity of antibodies<sup>19</sup>.

356 Taken together, these data indicate that VIR-7831 and VIR-7832 can play a powerful role in the fight  
357 against COVID-19 through the dual action of broadly neutralizing activity paired with engagement of the  
358 immune system through effector function capabilities.

359

## 360 **METHODS**

361 **Cells.** Vero E6 cells (ATCC) and Lenti-X 293T cells (Takara) were cultured in Dulbecco's Modified  
362 Eagle's medium (DMEM), 10% FBS, 1x Penicillin-Streptomycin at 37°C, 5% CO<sub>2</sub>.

363 **Monoclonal Antibodies.** VIR-7831 and VIR-7832 were produced at WuXi Biologics (China). SGHmAb-  
364 no-LS, S309-LS, and S309-GRLR were produced at Humabs Biomed SA, a subsidiary of Vir  
365 Biotechnology (Bellinzona, Switzerland) in expiCHO cells transiently co-transfected with plasmids  
366 expressing the heavy and light chain, as previously described <sup>62</sup>

367 **Virus.** SARS-CoV-2 isolates USA-WA1/2020, UK/VUI/3/2020, hCoV-19/South Africa/KRISP-  
368 K005325/2020, hCoV-19/Japan/TY7-503/2021, hCoV-19/USA/CA-SU-15-S02/2021 and hCoV-



369 19/USA/PHC658/2021 were obtained from BEI Resources. To propagate SARS-CoV-2, VeroE6 or  
370 VeroE6-TMPRSS2 cells were seeded at  $10 \times 10^6$  cells in T175 flasks in growth media and infected the  
371 next day at a MOI of 0.001 in virus propagation media. Virus was adsorbed for 1 hour at 37°C. Virus  
372 inoculum was removed, flasks were washed once with PBS, 25 mL of infection media was added to the  
373 cells and flasks were incubated at 37°C. Supernatants were collected at 48 hours post-infection once  
374 cytopathic effect was visible, centrifuged at 500 x g for 5 minutes, followed by a second centrifugation at  
375 1000 x g for 5 minutes. Clarified supernatants were then aliquoted and stored at -80°C. Virus titers were  
376 determined using a plaque assay on VeroE6 cells, using standard methods. Briefly, 10-fold dilutions of  
377 virus stock were incubated in 6 well plates with 2.4% colloidal cellulose overlay for 24 hours. Cells were  
378 fixed with 4% PFA for 30 minutes at room temperature (RT), permeabilized with 0.125% Triton X-100,  
379 stained with anti-SARS-CoV-2 nucleocapsid antibody at 1:5000 and goat anti-rabbit IgG HRP at 1:5000.  
380 Plaque forming units (PFU) were visualized with TrueBlue reagent.

381 **In vitro binding ELISA.** For the ELISA assay, 96-well plates were coated with 100 µl/well recombinant  
382 SARS-CoV2 RBD diluted in assay diluent (1% BSA/PBS) at a final concentration of 2 µg/mL and  
383 incubated overnight at 4°C. Plates were washed three times with 300 µl/well wash buffer using an  
384 automated washer. Assay diluent (100 µl/well) was added to block the plates and incubated for 1 hour at  
385 room temperature (RT) with shaking. Assay diluent was removed, and plates washed three times with  
386 wash buffer. Serial 1:3 dilutions of mAb (concentration range from 6 µg/mL to 0.33 ng/mL) in assay  
387 diluent were dispensed at 100 µl/well and incubated 1 hour at RT with shaking, then washed three times  
388 with wash buffer. The HRP-conjugated secondary antibody reagent (1:5,000 dilution in assay diluent)  
389 was added to each well (100 µl/well) and incubated for 1 hour at RT with shaking. After three washes  
390 with wash buffer, 100 µl/well of 2-component TMB peroxidase substrate solution was dispensed in each  
391 well and developed for 5 minutes at RT. The reaction was stopped with 100 µL/well 1M H<sub>2</sub>SO<sub>4</sub> and the  
392 OD was read immediately at 450 nm on a SpectraMax M5 Microplate reader. EC<sub>50</sub> values were calculated  
393 using non-linear regression of log (agonist) versus response in Graph Pad Prism.



394 **Spike binding affinity quantification by SPR.** Antibody was diluted to 2 µg/mL (1 mL) in HBS-EP+  
395 buffer and injected at 10 µL/min for 30 seconds across one flow cell of a CM5 sensor chip immobilized  
396 with anti-human Fc antibody docked in a Biacore T200. SARS-CoV2-RBD diluted in HBS-EP+ buffer  
397 was then injected at a single concentration, 1:3 dilutions from 100 nM to 3.7 nM, across both the flow cell  
398 containing captured the antibody as well as a reference flow cell containing only anti-human Fc antibody.  
399 Binding was measured with a flow rate of 30 µL/min and an injection time of 600 seconds; dissociation  
400 was monitored for 1800 seconds after injection. Data were collected at 10 Hz. After each binding  
401 measurement, regeneration reagent was injected to prepare the surface for a new cycle. Experiments were  
402 performed at 25°C, with the samples held at 15 °C in the instrument prior to injection.

403 **Measurement of Binding to Human Fcγ Receptors by SPR.** Binding of VIR-7831 and VIR-7832 to  
404 human recombinant FcγRs was measured by surface plasmon resonance (SPR) on a Biacore T200.  
405 Briefly, Biotin CAPture Reagent (modified streptavidin) was injected across all flow cells of a CAP  
406 sensor chip docked in a Biacore T200. Biotinylated Fc receptors at 1 µg/mL were injected across a single  
407 flow cell at 10 µL/min for 60 seconds (one receptor per flow cell), with one flow cell reserved as a  
408 reference surface. VIR 7831 or VIR-7832 at 100 µg/mL (diluted in HBS-EP+) were injected across all  
409 flow cells for 200 seconds using a flow rate of 30 µL/min and association was monitored. Dissociation  
410 was monitored for another 200 seconds after injection. Data was collected at 10 Hz. After each binding  
411 measurement, CAP Regeneration reagent was injected to prepare the surface for a new cycle.  
412 Experiments were performed at 25°C, with the samples held at 15°C in the instrument prior to injection.

413 **Measurement of Binding to Human Complement Protein C1q.** Binding of VIR-7831 and VIR-7832 to  
414 human complement was measured by biolayer interferometry (BLI) using an Octet Red96 instrument  
415 (FortéBio). Briefly, anti-human Fab (CH1-specific) sensors were used to capture VIR-7831 and VIR-  
416 7832 at 10 µg/ml for 10 minutes. The IgG-loaded sensors were then exposed to kinetics buffer containing  
417 3 µg/ml of purified human C1q for 4 minutes, followed by a dissociation step in the same buffer for

418 additional 4 minutes. Association and dissociation profiles were measured in real time as changes in the  
419 interference pattern.

420 **Binding to Cell Surface Expressed SARS-CoV-2 Spike Protein.** The SARS-CoV-2 spike protein  
421 coding sequence (YP\_009724390.1, Wuhan-Hu-1 strain) was cloned into a cell expression plasmid under  
422 the control of the human CMV promoter (phCMV1) to generate phCMV1 WT spike. ExpiCHO-S cells  
423 were seeded the day before transfection at  $3 \times 10^6$  cells/mL in ExpiCHO Expression Medium.  
424 Immediately before transfection, the cells were seeded at  $6 \times 10^6$  cells/mL in a volume of 15 mL in  
425 125 mL shake flasks. Six  $\mu\text{g}$  of phCMV1 WT spike plasmid or vector control were diluted in 1.2 mL of  
426 iced OptiPRO SFM., followed by addition of 48  $\mu\text{L}$  of ExpiFectamine CHO Reagent and complexing for  
427 1 minute at RT. The transfection mixture was added dropwise to cells with gentle swirling. Cells were  
428 then incubated at  $37^\circ\text{C}$ , 8%  $\text{CO}_2$  with shaking for 42 hours. At 42 hours post-transfection, ExpiCHO-S  
429 cells were harvested, washed twice with FACS buffer and resuspended at a concentration of  $1.0 \times 10^6$   
430 cell/mL in PBS. Cells ( $5 \times 10^4$  cells in 50  $\mu\text{L}$ /wells) were dispensed into a 96-well V-bottom plate.  
431 Antibody was serially diluted (1:4, 10 points) starting at a concentration of 10  $\mu\text{g}/\text{mL}$ . Cells were pelleted  
432 at  $300 \times g$  for 5 minutes and resuspended in 50  $\mu\text{L}$ /well of antibody serial dilutions and plates were  
433 incubated for 45 mins on ice. Cells were washed twice in FACS buffer. Alexa Fluor 647-labelled Goat  
434 Anti-Human IgG secondary Ab was diluted 1:750 in FACS buffer and 50  $\mu\text{L}$  was added to the cell pellet  
435 for 15 min on ice. Cells were washed twice with FACS buffer, resuspended in 1% PFA. Data was  
436 acquired by flow cytometry (CytoFlex LX).

437 **Pseudotyped virus production.** Lenti-X<sup>TM</sup> 293T cells were seeded in 10-cm dishes for 80% next day  
438 confluency. The next day, cells were transfected with the plasmid pcDNA3.1(+)-spike-D19 (encoding the  
439 SARS-CoV-2 spike protein) or pcDNA3.1(+)-spike-D19 variants using the transfection reagent TransIT-  
440 Lenti according to the manufacturer's instructions. One day post-transfection, cells were infected with  
441 VSV-luc (rVSV $\Delta\text{G}$ ; Kerafast) at an MOI of 3. The cell supernatant containing SARS-CoV-2 pseudotyped

442 virus was collected at day 2 post-transfection, centrifuged at 1000 x g for 5 minutes to remove cellular  
443 debris, aliquoted and frozen at -80°C.

444 **In Vitro Neutralization of SARS-CoV-2 Pseudotyped Virus.** VeroE6 cells were seeded into flat  
445 bottom tissue culture 96-well plates at 20,000 cells/well and cultured overnight at 37°C. Twenty-four  
446 hours later, 9-point 1:4 serial dilutions of VIR-7831 were prepared in infection medium and each dilution  
447 was tested in triplicate per plate (range: 20,000 to 0.3 ng/mL final concentration). SARS-CoV-2 virus  
448 stock was diluted in infection media for a final concentration of 2000 plaque forming units per well (MOI  
449 0.1). Antibody dilutions were added to virus and incubated for 30 minutes at 37°C. Media was removed  
450 from the VeroE6 cells, mAb-virus complexes were added, and cells were incubated at 37°C. At 6 hours  
451 post-infection, cells were fixed with 250 µL 4% PFA, incubated for 30 minutes at RT, then washed 3  
452 times with PBS to remove residual PFA. The cells were permeabilized with 50 µL of 0.125% Triton X-  
453 100 in PBS for 30 minutes at RT. The blocking buffer was removed, 50 µL of SARS-CoV-2 nucleocapsid  
454 antibody at 1:2,000 in blocking buffer was added, and plate was incubated for 1 hour at RT. Plates were  
455 washed three times with PBS and then incubated for 1 hour at RT with 50 µL/well of goat anti-rabbit-  
456 Alexa647 secondary antibody at a final dilution of 1:1,000 mixed with 2 ug/mL Hoechst dye in blocking  
457 buffer. After washing 5 times with PBS, 100 µL of fresh PBS was added for imaging. Plates were imaged  
458 on a Cytation5 plate reader. Whole well images were acquired (12 images at 4X magnification per well)  
459 and nucleocapsid-positive cells were counted using the manufacturer's software.

460 **Live virus neutralization.** VeroE6 cells were seeded into flat bottom tissue culture 96-well plates at  
461 20,000 cells/well and cultured overnight at 37°C. Twenty-four hours later, 9-point 1:4 serial dilutions of  
462 VIR-7831 were prepared in infection medium and each dilution was tested in triplicate per plate (range:  
463 20,000 to 0.3 ng/mL final concentration). SARS-CoV-2 virus stock was diluted in infection media for a  
464 final concentration of 2000 plaque forming units per well (MOI 0.1). Antibody dilutions were added to  
465 virus and incubated for 30 minutes at 37°C. Media was removed from the VeroE6 cells, mAb-virus  
466 complexes were added, and cells were incubated at 37°C. At 6 hours post-infection, cells were fixed with

467 250  $\mu$ L 4% PFA, incubated for 30 minutes at RT, then washed 3 times with PBS to remove residual PFA.  
468 The cells were permeabilized with 50  $\mu$ L of 0.125% Triton X-100 in PBS for 30 minutes at RT. The  
469 blocking buffer was removed, 50  $\mu$ L of SARS-CoV-2 nucleocapsid antibody at 1:2,000 in blocking buffer  
470 was added, and plate was incubated for 1 hour at RT. Plates were washed three times with PBS and then  
471 incubated for 1 hour at RT with 50  $\mu$ L/well of goat anti-rabbit-Alexa647 secondary antibody at a final  
472 dilution of 1:1,000 mixed with 2  $\mu$ g/mL Hoechst dye in blocking buffer. After washing 5 times with PBS,  
473 100  $\mu$ L of fresh PBS was added for imaging. Plates were imaged on a Cytation5 plate reader. Whole well  
474 images were acquired (12 images at 4X magnification per well) and nucleocapsid-positive cells were  
475 counted using the manufacturer's software..

476 **Determination of Viral Titer by Focus-Forming Assay.** One day prior to infection,  $1.2 \times 10^4$  VeroE6  
477 cells were plated in black-walled, clear bottomed 96-well plates. Virus samples were diluted 1:5 in  
478 infection media and adsorbed onto VeroE6 cells for one hour at 37°C. The cells were washed once and  
479 overlaid with 1% methylcellulose/serum-containing media. At 24 hours post-infection, the  
480 methylcellulose overlay was removed, and cells were washed with PBS. Cells were fixed with 4% PFA,  
481 incubated for 30 minutes at RT, then washed with PBS to remove residual PFA. The cells were  
482 permeabilized with 50  $\mu$ L of 0.25% Triton X-100 in PBS for 30 minutes at RT. The Triton X-100 was  
483 removed, cells were washed twice with PBS, and incubated with 50  $\mu$ L of SARS-CoV-2 nucleocapsid  
484 antibody at 1:2,000 in blocking buffer for one hour at RT. Plates were washed three times with PBS and  
485 then incubated for one hour at RT with 50  $\mu$ L/well of goat anti-rabbit-Alexa647 secondary antibody at  
486 1:1,000 in blocking buffer. After washing three times with PBS, 50  $\mu$ L of Hoechst dye at 1:1,000 in PBS  
487 was added for imaging. Plates were imaged on a Cytation5 plate reader. Whole well images were  
488 acquired (12 images at 4X magnification per well) and nucleocapsid-positive foci were counted using the  
489 manufacturer's software and used to determine focus-forming units/mL supernatant (FFU/mL).

490 **Determination of mAb-Dependent Activation of Human Fc $\gamma$ RIIIa, Fc $\gamma$ RIIIa or Fc $\gamma$ RIIb.** VIR-7831,  
491 VIR-7832, S309-LS, and a control mAb with abrogated Fc $\gamma$ R binding, S309-GRLR, were serially diluted

492 6-fold in assay buffer from 10,000 ng/ml to 0.006 ng/ml. Nine-point serial dilutions of mAbs were  
493 incubated with 12,500 (for Fc $\gamma$ RIIIa and Fc $\gamma$ RIIb) or 10,000 (for Fc $\gamma$ RIIIa) CHO-CoV-2-Spike cells per  
494 96-plate well in a white, flat-bottom plate for 15 minutes at room temperature. Jurkat effector cells  
495 expressing indicated Fc $\gamma$ Rs and stably transfected with an NFAT-driven luciferase gene were thawed,  
496 diluted in assay buffer, and added to the plate at an effector to target cell ratio of 6:1 for Fc $\gamma$ RIIIa and  
497 Fc $\gamma$ RIIb or 5:1 for Fc $\gamma$ IIa. Control wells were also included that were used to measure antibody-  
498 independent activation (containing target cells and effector cells but no antibody) and background  
499 luminescence of the plate (wells containing assay buffer only). Plates were incubated for 18 hours at 37°C  
500 with 5% CO<sub>2</sub>. Activation of human Fc $\gamma$ Rs in this bioassay results in the NFAT-mediated expression of  
501 the luciferase reporter gene. Luminescence was measured with a luminometer after adding the Bio  
502 GloTM Luciferase Assay Reagent according to the manufacturer's instructions. To control for  
503 background, the mean of the relative luminescence units (RLU) values in wells containing only Assay  
504 Buffer was calculated and subtracted from all data points. Data were expressed as the average of RLUs  
505 over the background

506 **Determination of NK-Cell Mediated Antibody-Dependent Cellular Cytotoxicity.** Primary NK cell  
507 activation was tested using freshly isolated cells from two previously genotyped donors expressing  
508 homozygous low affinity (F158) or high affinity (V158) Fc $\gamma$ RIIIa. Serial dilutions of mAbs (serially  
509 diluted 10-fold in AIM-V Medium from 40,000 ng/ml to 0.075 ng/ml) were incubated with 7,500 CHO-  
510 CoV-2 Spike cells per well of a 96 well round-bottom plate for 10 minutes. Target cell and antibody  
511 mixtures were then incubated with primary human NK cells as effectors at an effector-to-target ratio of  
512 10:1. ADCC was measured using lactate dehydrogenase (LDH) release as a readout according to the  
513 manufacturer's instructions (Cytotoxicity Detection Kit (LDH), Roche) after 4 hours of incubation at  
514 37°C. In brief, plates were centrifuged for 4 minutes at 400 x g, and 35  $\mu$ l of supernatant was transferred  
515 to a flat 384 well plate. LDH reagent was prepared and 35  $\mu$ l were added to each well. Using a kinetic  
516 protocol, the absorbance at 490 nm and 650 nm was measured once every 2 minutes for 8 minutes, and

517 the slope of the kinetics curve was used as result. The percent specific lysis was determined by applying  
518 the following formula: (specific release – spontaneous release) / (maximum release - spontaneous release)  
519 x 100.

520 **Determination of Monocyte-Mediated Antibody-Dependent Cellular Phagocytosis.** ADCP assays  
521 were performed using human PBMCs freshly isolated from whole blood. CHO CoV-2-Spike cells were  
522 used as target cells and were fluorescently labeled with PKH67 Fluorescent Cell Linker Kit (Sigma  
523 Aldrich) prior to incubation with mAbs, according to manufacturer's instructions. Serial dilutions of  
524 mAbs (serially diluted 5-fold from 5,000 ng/ml to 0.32 ng/ml in RPMI-1640 + L-glutamine supplemented  
525 with 10% Hyclone FBS + 2x anti-anti (antibiotic-antimycotic)) were incubated with 10,000 CHO-CoV-2-  
526 Spike cells per well of a 96 well polypropylene plate for 10 minutes. Primary PBMCs were fluorescently  
527 labeled with Cell Trace Violet according to the manufacturer's instructions. Target cell and antibody  
528 mixtures were then incubated with labeled PBMCs at an effector-to-target ratio of 16:1. After an  
529 overnight incubation at 37°C, monocytes were stained with anti-human CD14-APC antibody (BD  
530 Pharmingen). Antibody-mediated phagocytosis was determined by flow cytometry, gating on CD14+  
531 cells that were double positive for cell trace violet and PKH67. Raw data were exported from the flow  
532 cytometer into the flow cytometry analysis software FlowJo v10 (Becton Dickinson) for gating and  
533 determination of the percentage of CD14<sup>+</sup> cells that were also double positive for cell trace violet and  
534 PKH67. Cells expressing only cell trace violet or only PKH67 were used to set the positive staining gates.

535 **In vitro resistance selection.** The selection of variants in the presence of increasing concentrations of  
536 VIR-7832 was conducted in VeroE6 cells. The day before infection, 6 x 10<sup>4</sup> VeroE6 cells were seeded in  
537 24 well plates and incubated overnight at 37°C. The next day, 600 focus forming units (FFU) of SARS-  
538 CoV-2 virus (MOI = 0.01) was incubated with 0.5X IC<sub>50</sub> of VIR-7832 (0.05 µg/mL) at 37°C for one hour  
539 in infection media. The mAb-virus complexes were adsorbed on VeroE6 cells for one hour at 37°C in  
540 duplicate wells. After adsorption, cells were washed with DMEM and overlaid with infection media  
541 containing 0.05 µg/mL VIR-7832. Control wells infected without antibody were included with each

542 passage. Infected cells were monitored visually for CPE daily. In general, when infected cells exhibited  $\geq$   
543 50% CPE, the culture supernatants were harvested, diluted 1:200, and added to fresh VeroE6 cells in 24-  
544 well plates with equivalent or increasing concentrations of VIR-7832. At each passage, supernatant was  
545 aliquoted and frozen at  $-80^{\circ}\text{C}$  for titer and neutralization analyses.

546 **In vitro assessment of potential for ADE.** VeroE6 cells were plated at  $1.25 \times 10^4$  cells/well one day prior  
547 to infection. For each independent experiment, moDCs and PBMCs from five unique moDC donors and  
548 six unique PBMC donors were used, with three unique donors used for each independent experiment.  
549 Cryopreserved monocytes from unique donors were differentiated into moDCs for six days using human  
550 moDC differentiation media according to the manufacturer's protocol. Cryopreserved PBMCs from  
551 unique donors are thawed in the presence 0.3 mg/mL DNase and cultured in media for one day prior to  
552 infection. On the day of infection, moDCs, PBMCs, and U937 cells were counted and plated at  $7.5 \times 10^4$   
553 cells/well.

554 To examine viral entry, 24 hours post-infection, cells were fixed with 4% PFA, incubated for 30 minutes  
555 at RT, then washed with PBS to remove residual PFA. The cells were permeabilized with 50  $\mu\text{L}$  of 0.25%  
556 Triton X-100 in PBS for 30 minutes at RT. The Triton X-100 was removed, cells were washed twice with  
557 PBS, and incubated with 50  $\mu\text{L}$  of SARS-CoV-2 nucleocapsid antibody at 1:2,000 in blocking buffer for  
558 one hour at RT. Plates were washed three times with PBS and then incubated for one hour at RT with 50  
559  $\mu\text{L}$ /well of goat anti-rabbit-Alexa647 secondary antibody at 1:1,000 in blocking buffer. After washing  
560 three times with PBS, 50  $\mu\text{L}$  of Hoechst dye at 1:1,000 in PBS was added for imaging. Plates were  
561 imaged on a Cytation5 plate reader. Whole well images were acquired (12 images at 4X magnification  
562 per well) and nucleocapsid-positive cells were counted using the manufacturer's software. The percent of  
563 nucleocapsid+ cells was quantified using the Gen5 Imager software (Biotek, Vermont) as number of  
564 Cy5+ cells,  $[(\text{nucleocapsid+ cells})/\text{number of Hoechst+ cells (total cells)}] \times 100$ . Data was analyzed using  
565 Prism v8.00 (GraphPad Software, La Jolla California USA, [www.graphpad.com](http://www.graphpad.com)).



566 In order to quantify chemokines and cytokines from supernatants in a BSL2 laboratory, supernatants were  
567 inactivated by 10 minutes exposure to UVC light at 5,000  $\mu\text{J}/\text{cm}^2$ . Supernatants were diluted 1:5 in  
568 infection media and levels of cytokines/chemokines were quantified using the U-plex 96-well assay  
569 according to the manufacturer's protocol (Meso Scale Diagnostics, Rockville, MD). Quantification of  
570 cytokines and chemokines were determined based on an 8-point standard curve in duplicate, provided by  
571 the manufacturer. Cytokine data was analyzed using the Discovery Workbench v4.0.13 software (Meso  
572 Scale Diagnostics). Data was graphed and statistical analyses were conducted using Prism software.

573 **Sequencing of SARS-CoV-2 Spike Gene.** To isolate nucleic acid from the supernatant of viral passages,  
574 120  $\mu\text{L}$  of cell supernatant was added to 360  $\mu\text{L}$  of Trizol and stored at  $-80^\circ\text{C}$  for further analysis. Trizol  
575 collected samples from viral passages where a shift in neutralization  $> 2$ -fold relative to wild type was  
576 detected were subjected to RNA isolation using PureLink RNA Mini Kit with the incorporation of on-  
577 column PureLink DNase Treatment, following manufacturer's instructions. Reverse transcription  
578 reactions were performed with 6  $\mu\text{L}$  of purified RNA and oligoT primers using the NEB ProtoScript II  
579 First Strand cDNA Synthesis kit, according to manufacturer's instructions. The resulting cDNA was used  
580 as a template for PCR amplification of the spike gene using the KapaBiosystems polymerase (KAPA HiFi  
581 HotStart ReadyMix) with primers 5' aattatcttgcaaacacg-3' and 5' tgaggcttgatcggtatcg-3'.  
582 Amplification conditions included an initial 3 minutes at  $95^\circ\text{C}$ , followed by 28 cycles with 20 seconds at  
583  $98^\circ\text{C}$ , 15 seconds at  $62^\circ\text{C}$  and  $72^\circ\text{C}$  for 2 minutes, with a final 4 minutes at  $72^\circ\text{C}$ . PCR products were  
584 purified using AMPure XP beads following manufacturer's instructions. The size of the amplicon was  
585 confirmed by analyzing 2  $\mu\text{L}$  of PCR products using the Agilent D5000 ScreenTape System. Products  
586 were quantified by analyzing 1  $\mu\text{L}$  with the Quant-iT dsDNA High-Sensitivity Assay Kit. Twenty ng of  
587 purified PCR product was used as input for library construction using the NEBNext Ultra II FS DNA  
588 Library Prep kit following manufacturer's instructions. DNA fragmentation was performed for 13  
589 minutes. NEBNext Multiplex Oligos for Illumina Dual Index Primer Set 1 was used for library  
590 construction, with a total of 6 PCR cycles. Libraries size was determined using the Agilent D1000



591 ScreenTape System and quantified with the Quant iT dsDNA High-Sensitivity Assay Kit. Equal amounts  
592 of each library were pooled together for multiplexing and ‘Protocol A: Standard Normalization Method’  
593 of the Illumina library preparation guide was used to prepare 8 pM final multiplexed libraries with 1%  
594 PhiX spike-in for sequencing. The MiSeq Reagent Kit v3 (600-cycle) was used for sequencing the  
595 libraries on the Illumina MiSeq platform, with 300 cycles for Read 1, 300 cycles for Read 2, 8 cycles for  
596 Index 1, and 8 cycles for Index 2.

597 **Bioinformatics Analysis of Conservation.** Available genome sequences for SARS-CoV-2 were  
598 downloaded from Global Initiative on Sharing All Influenza Data (GISAID; <https://www.gisaid.org/>) on  
599 June 4, 2021. Bat and pangolin sequences were removed to yield human-only sequences. The spike open  
600 reading frame was localized by aligning the reference protein sequence (NCBI reference sequence:  
601 YP\_009724390.1) to the genomic sequence of isolates with Exonerate v.2.4.0. Coding nucleotide  
602 sequences were translated in silico using seqkit v.0.12.0. Multiple sequence alignment was performed  
603 using MAFFT v.7.455. Variants were determined by comparison of aligned sequences to the reference  
604 sequence using the R v3.6.3/Bioconductor v.3.10 package Biostrings v.2.54.0.

605 **In vivo studies.** Syrian golden hamster studies were conducted at Lovelace Biomedical (Albuquerque,  
606 NM). Twelve- to sixteen-week-old male hamsters were interperitoneally administered a non-LS version  
607 of VIR-7831 (SGHmAb-no-LS), control antibody or diluent Day -1 or Day -2 prior to virus challenge.  
608 Animals were inoculated intranasally at Day 0 with  $7.4 \times 10^4$  TCID<sub>50</sub> with SARS-CoV-2 (isolate USA-  
609 WA1/2020). Animals were also weighed once daily in the morning beginning on study Day -10 and  
610 continuing until the end of the study. Following euthanasia, RT-qPCR was performed on lung  
611 homogenates using quantitative real-time PCR methods targeting the SARS-CoV-2 N gene and the  
612 median tissue culture infections dose (TCID<sub>50</sub>) was determined per Lovelace internal methodology.

### 613 **Author Contributions**

614 Conceived studies: A.L.C, C.H-D., F.A.P, D.M., M.S., L.S., A.T., L.A.P., S.H., G.S., H.W.V., D.C., C.M.H.  
615 Designed studies and experiments: A.L.C, C.H.D., F.A.P, D.M., M.S., M.L.A., E. D., B.G., J.D., L.R.,A.C., A.S.,

616 R.S., J.W., N.C., E.C., S.L., C.C., D.P., C.S., J.N., A.P., A.W., L.S., A.T., L.A.P., S.H., G.S., H.W.V., D.C., C.M.H.  
617 Performed experiments: D.M., M.S., M.L.A., B.G., J.D., E.D., A.S., L.R., H.T., J.D., S.S., D.P., C.S., J.N., B.S.,  
618 S.B., J.W., J.Z., H.K., A.C., M.M-R., A.P., A.W., N.C., E.C. Analyzed and interpreted data: A.L.C., C.H-D., F.A.L.,  
619 D.M., M.S., M.L.A., B.G., J.D., D.P., C.S., J.N., E.L., A.S., R.S., L.R., H.T., B.S., S.B., J.W., J.Z., H.K., A.C., M. M-  
620 R., N.C., E.C., S.L., A.W., C.C., L.S., A.T., S.H., G.S., H.W.G, D.C., C.M.H. Prepared the manuscript with input  
621 from all authors: A.L.C., G.S., A.T., L.P., D.C., H.W.G., C.M.H.

## 622 **Competing interests**

623 Some authors are current or former employees of Vir Biotechnology or Humabs BioMed SA (a fully-  
624 owned subsidiary of Vir Biotechnology) and may hold shares in Vir Biotechnology. H.W.V. is a founder of  
625 PierianDx and Casma Therapeutics. This research was sponsored and funded by Vir Biotechnology in  
626 collaboration with GSK.

627

628 **REFERENCES**

629

630 1. WHO Coronavirus Disease (COVID-19) Dashboard | WHO Coronavirus Disease (COVID-19)  
631 Dashboard. <https://covid19.who.int/>.

632 2. Levin, A. T. *et al.* Assessing the age specificity of infection fatality rates for COVID-19:  
633 systematic review, meta-analysis, and public policy implications. *Eur J Epidemiol* **35**, 1123–  
634 1138 (2020).

635 3. Dennis, A. *et al.* Multi-organ impairment in low-risk individuals with long COVID.  
636 doi:10.1101/2020.10.14.20212555.

637 4. Murphy, J. *et al.* Psychological characteristics associated with COVID-19 vaccine hesitancy  
638 and resistance in Ireland and the United Kingdom. *Nat Commun* **12**, 29 (2021).

639 5. Khubchandani, J. *et al.* COVID-19 Vaccination Hesitancy in the United States: A Rapid  
640 National Assessment. *J Commun Health* 1–8 (2021) doi:10.1007/s10900-020-00958-x.

641 6. Sallam, M. *et al.* High Rates of COVID-19 Vaccine Hesitancy and Its Association with  
642 Conspiracy Beliefs: A Study in Jordan and Kuwait among Other Arab Countries. *Nato Adv Sci*  
643 *Inst Se* **9**, 42 (2021).

644 7. Tegally, H. *et al.* Emergence and rapid spread of a new severe acute respiratory syndrome-  
645 related coronavirus 2 (SARS-CoV-2) lineage with multiple spike mutations in South Africa.  
646 *medRxiv* (2020) doi:10.1101/2020.12.21.20248640.

647 8. Naveca, F. *et al.* Phylogenetic relationship of SARS-CoV-2 sequences from Amazonas with  
648 emerging Brazilian variants harboring mutations E484K and N501Y in the Spike protein -  
649 SARS-CoV-2 coronavirus / nCoV-2019 Genomic Epidemiology - Virological.  
650 [https://virological.org/t/phylogenetic-relationship-of-sars-cov-2-sequences-from-amazonas-with-](https://virological.org/t/phylogenetic-relationship-of-sars-cov-2-sequences-from-amazonas-with-emerging-brazilian-variants-harboring-mutations-e484k-and-n501y-in-the-spike-protein/585)  
651 [emerging-brazilian-variants-harboring-mutations-e484k-and-n501y-in-the-spike-protein/585](https://virological.org/t/phylogenetic-relationship-of-sars-cov-2-sequences-from-amazonas-with-emerging-brazilian-variants-harboring-mutations-e484k-and-n501y-in-the-spike-protein/585)  
652 (2021).

653 9. Rambaut, A. *et al.* Preliminary genomic characterisation of an emergent SARS-CoV-2 lineage  
654 in the UK defined by a novel set of spike mutations - SARS-CoV-2 coronavirus / nCoV-2019  
655 Genomic Epidemiology - Virological. [https://virological.org/t/preliminary-genomic-](https://virological.org/t/preliminary-genomic-characterisation-of-an-emergent-sars-cov-2-lineage-in-the-uk-defined-by-a-novel-set-of-spike-mutations/563)  
656 [characterisation-of-an-emergent-sars-cov-2-lineage-in-the-uk-defined-by-a-novel-set-of-spike-](https://virological.org/t/preliminary-genomic-characterisation-of-an-emergent-sars-cov-2-lineage-in-the-uk-defined-by-a-novel-set-of-spike-mutations/563)  
657 [mutations/563](https://virological.org/t/preliminary-genomic-characterisation-of-an-emergent-sars-cov-2-lineage-in-the-uk-defined-by-a-novel-set-of-spike-mutations/563) (2020).

658 10. Bamlanivimab EUA Letter of Authorization Reissue 02092021.  
659 <https://www.fda.gov/media/143603/download>.

660 11. Casirivimab and Imdevimab EUA Fact Sheet for Healthcare Providers.  
661 <https://www.fda.gov/media/143892/download>.

- 662 12. Lilly's neutralizing antibody bamlanivimab (LY-CoV555) prevented COVID-19 at nursing  
663 homes in the BLAZE-2 trial, reducing risk by up to 80 percent for residents.  
664 <https://investor.lilly.com/node/44291/pdf>.
- 665 13. Gottlieb, R. L. *et al.* Effect of Bamlanivimab as Monotherapy or in Combination With  
666 Etesevimab on Viral Load in Patients With Mild to Moderate COVID-19. *Jama* **325**, 632–644  
667 (2021).
- 668 14. Chen, P. *et al.* SARS-CoV-2 Neutralizing Antibody LY-CoV555 in Outpatients with Covid-  
669 19. *New Engl J Med* (2020) doi:10.1056/nejmoa2029849.
- 670 15. Weinreich, D. M. *et al.* REGN-COV2, a Neutralizing Antibody Cocktail, in Outpatients with  
671 Covid-19. *New Engl J Med* **384**, 238–251 (2020).
- 672 16. Gupta, A. *et al.* Early Treatment for Covid-19 with SARS-CoV-2 Neutralizing Antibody  
673 Sotrovimab. *New Engl J Med* **385**, 1941–1950 (2021).
- 674 17. Starr, T. N. *et al.* Prospective mapping of viral mutations that escape antibodies used to treat  
675 COVID-19. *Science* **371**, 850–854 (2021).
- 676 18. Wang, P. *et al.* Increased Resistance of SARS-CoV-2 Variants B.1.351 and B.1.1.7 to  
677 Antibody Neutralization. *Biorxiv* 2021.01.25.428137 (2021) doi:10.1101/2021.01.25.428137.
- 678 19. Schäfer, A. *et al.* Antibody potency, effector function, and combinations in protection and  
679 therapy for SARS-CoV-2 infection in vivo. *J Exp Med* **218**, (2020).
- 680 20. Winkler, E. S. *et al.* Human neutralizing antibodies against SARS-CoV-2 require intact Fc  
681 effector functions and monocytes for optimal therapeutic protection. *Biorxiv* 2020.12.28.424554  
682 (2020) doi:10.1101/2020.12.28.424554.
- 683 21. Bournazos, S. & Ravetch, J. V. Fcγ Receptor Function and the Design of Vaccination  
684 Strategies. *Immunity* **47**, 224–233 (2017).
- 685 22. Pinto, D. *et al.* Cross-neutralization of SARS-CoV-2 by a human monoclonal SARS-CoV  
686 antibody. *Nature* **583**, 290–295 (2020).
- 687 23. Pinto, D. *et al.* Cross-neutralization of SARS-CoV-2 by a human monoclonal SARS-CoV  
688 antibody. *Nature* **583**, 290–295 (2020).
- 689 24. Ko, S.-Y. *et al.* Enhanced neonatal Fc receptor function improves protection against primate  
690 SHIV infection. *Nature* **514**, 642 (2014).
- 691 25. Zalevsky, J. *et al.* Enhanced antibody half-life improves in vivo activity. *Nat Biotechnol* **28**,  
692 157 (2010).

- 693 26. Gaudinski, M. R. *et al.* Safety and pharmacokinetics of the Fc-modified HIV-1 human  
694 monoclonal antibody VRC01LS: A Phase 1 open-label clinical trial in healthy adults. *Plos Med*  
695 **15**, e1002493 (2018).
- 696 27. Bournazos, S., Corti, D., Virgin, H. W. & Ravetch, J. V. Fc-optimized antibodies elicit CD8  
697 immunity to viral respiratory infection. *Nature* 1–9 (2020) doi:10.1038/s41586-020-2838-z.
- 698 28. Weitzenfeld, P., Bournazos, S. & Ravetch, J. V. Antibodies targeting sialyl Lewis A mediate  
699 tumor clearance through distinct effector pathways. *J Clin Invest* **129**, 3952–3962 (2019).
- 700 29. Bournazos, S., Corti, D., Virgin, H. W. & Ravetch, J. V. Fc-optimized antibodies elicit CD8  
701 immunity to viral respiratory infection. *Nature* 1–9 (2020) doi:10.1038/s41586-020-2838-z.
- 702 30. Diamond, M. *et al.* SARS-CoV-2 variants show resistance to neutralization by many  
703 monoclonal and serum-derived polyclonal antibodies. *Res Square* (2021) doi:10.21203/rs.3.rs-  
704 228079/v1.
- 705 31. GISAID. <https://www.epicov.org/epi3>.
- 706 32. Stanford Covid Database. <https://covdb.stanford.edu/page/susceptibility-data>.
- 707 33. NCATS Database. <https://opendata.ncats.nih.gov/variant/activity>.
- 708 34. Kallewaard, N. L. *et al.* Structure and Function Analysis of an Antibody Recognizing All  
709 Influenza A Subtypes. *Cell* **166**, 596–608 (2016).
- 710 35. DiLillo, D. J., Tan, G. S., Palese, P. & Ravetch, J. V. Broadly neutralizing hemagglutinin  
711 stalk-specific antibodies require FcγR interactions for protection against influenza virus in vivo.  
712 *Nat Med* **20**, 143–151 (2014).
- 713 36. Dunand, C. J. H. *et al.* Both Neutralizing and Non-Neutralizing Human H7N9 Influenza  
714 Vaccine-Induced Monoclonal Antibodies Confer Protection. *Cell Host Microbe* **19**, 800–813  
715 (2016).
- 716 37. Leon, P. E. *et al.* Optimal activation of Fc-mediated effector functions by influenza virus  
717 hemagglutinin antibodies requires two points of contact. *Proc National Acad Sci* **113**, E5944–  
718 E5951 (2016).
- 719 38. Bruhns, P. *et al.* Specificity and affinity of human Fcγ receptors and their polymorphic  
720 variants for human IgG subclasses. *Blood* **113**, 3716–3725 (2009).
- 721 39. Weitzenfeld, P., Bournazos, S. & Ravetch, J. V. Antibodies targeting sialyl Lewis A mediate  
722 tumor clearance through distinct effector pathways. *J Clin Invest* **129**, 3952–3962 (2019).

- 723 40. Cheng, Z. J. *et al.* Development of a robust reporter-based ADCC assay with frozen, thaw-  
724 and-use cells to measure Fc effector function of therapeutic antibodies. *J Immunol Methods* **414**,  
725 69–81 (2014).
- 726 41. Arvin, A. M. *et al.* A perspective on potential antibody-dependent enhancement of SARS-  
727 CoV-2. *Nature* 1–11 (2020) doi:10.1038/s41586-020-2538-8.
- 728 42. Joyner, M. J. & Wright, R. S. Safety Update: CO VID-19 Convalescent Plasma in  
729 20,000 Hospitalized Patients. *Mayo Clinic Proceedings* (2020).
- 730 43. Arvin, A. M. *et al.* A perspective on potential antibody-dependent enhancement of SARS-  
731 CoV-2. *Nature* **584**, 353–363 (2020).
- 732 44. Khurana, S. *et al.* Vaccine-induced anti-HA2 antibodies promote virus fusion and enhance  
733 influenza virus respiratory disease. *Sci Transl Med* **5**, 200ra114 (2013).
- 734 45. Winarski, K. L. *et al.* Antibody-dependent enhancement of influenza disease promoted by  
735 increase in hemagglutinin stem flexibility and virus fusion kinetics. *Proc National Acad Sci* **116**,  
736 15194–15199 (2019).
- 737 46. Hui, K. P. Y. *et al.* Tropism, replication competence, and innate immune responses of the  
738 coronavirus SARS-CoV-2 in human respiratory tract and conjunctiva: an analysis in ex-vivo and  
739 in-vitro cultures. *Lancet Respir Medicine* (2020) doi:10.1016/s2213-2600(20)30193-4.
- 740 47. Liu, Z. *et al.* Identification of Common Deletions in the Spike Protein of Severe Acute  
741 Respiratory Syndrome Coronavirus 2. *J Virol* **94**, (2020).
- 742 48. Baum, A. *et al.* Antibody cocktail to SARS-CoV-2 spike protein prevents rapid mutational  
743 escape seen with individual antibodies. *Science* **369**, 1014–1018 (2020).
- 744 49. Thomson, E. C. *et al.* Circulating SARS-CoV-2 spike N439K variants maintain fitness while  
745 evading antibody-mediated immunity. *Cell* (2021) doi:10.1016/j.cell.2021.01.037.
- 746 50. Starr, T. N., Greaney, A. J., Dingens, A. S. & Bloom, J. D. Complete map of SARS-CoV-2  
747 RBD mutations that escape the monoclonal antibody LY-CoV555 and its cocktail with LY-  
748 CoV016. doi:10.1101/2021.02.17.431683.
- 749 51. Wise, J. Covid-19: The E484K mutation and the risks it poses. *Bmj* **372**, n359 (2021).
- 750 52. Chen, R. E. *et al.* Resistance of SARS-CoV-2 variants to neutralization by monoclonal and  
751 serum-derived polyclonal antibodies. *Nat Med* 1–10 (2021) doi:10.1038/s41591-021-01294-w.
- 752 53. VIR-7831 for the Early Treatment of COVID-19 in Outpatients - Full Text View -  
753 ClinicalTrials.gov. [https://clinicaltrials.gov/ct2/show/NCT04545060?term=VIR-](https://clinicaltrials.gov/ct2/show/NCT04545060?term=VIR-7831&draw=2&rank=2)  
754 [7831&draw=2&rank=2](https://clinicaltrials.gov/ct2/show/NCT04545060?term=VIR-7831&draw=2&rank=2).

- 755 54. A Study of Immune System Proteins in Participants With Mild to Moderate COVID-19  
756 Illness - Full Text View - ClinicalTrials.gov.  
757 <https://clinicaltrials.gov/ct2/show/NCT04634409?term=VIR-7831&draw=2&rank=3>.
- 758 55. Vir Biotechnology and GSK announce NHS-supported AGILE study to evaluate VIR-7832  
759 in the early treatment of COVID-19 | GSK. [https://www.gsk.com/en-gb/media/press-releases/vir-](https://www.gsk.com/en-gb/media/press-releases/vir-biotechnology-and-gsk-announce-nhs-supported-agile-study-to-evaluate-vir-7832-in-the-early-treatment-of-covid-19/)  
760 [biotechnology-and-gsk-announce-nhs-supported-agile-study-to-evaluate-vir-7832-in-the-early-](https://www.gsk.com/en-gb/media/press-releases/vir-biotechnology-and-gsk-announce-nhs-supported-agile-study-to-evaluate-vir-7832-in-the-early-treatment-of-covid-19/)  
761 [treatment-of-covid-19/](https://www.gsk.com/en-gb/media/press-releases/vir-biotechnology-and-gsk-announce-nhs-supported-agile-study-to-evaluate-vir-7832-in-the-early-treatment-of-covid-19/).
- 762 56. Starr, T. N. *et al.* SARS-CoV-2 RBD antibodies that maximize breadth and resistance to  
763 escape. *Nature* **597**, 97–102 (2021).
- 764 57. Starr, T. N. *et al.* SARS-CoV-2 RBD antibodies that maximize breadth and resistance to  
765 escape. *Nature* 1–9 (2021) doi:10.1038/s41586-021-03807-6.
- 766 58. CoVariants. <https://covariants.org/>.
- 767 59. Piccoli, L. *et al.* Mapping neutralizing and immunodominant sites on the SARS-CoV-2 spike  
768 receptor-binding domain by structure-guided high-resolution serology. *Cell* (2020)  
769 doi:10.1016/j.cell.2020.09.037.
- 770 60. Rappazzo, C. G. *et al.* Broad and potent activity against SARS-like viruses by an engineered  
771 human monoclonal antibody. *Science* **371**, 823–829 (2021).
- 772 61. Sette, A. & Crotty, S. Adaptive immunity to SARS-CoV-2 and COVID-19. *Cell* **184**, 861–  
773 880 (2021).
- 774 62. Stettler, K. *et al.* Specificity, cross-reactivity and function of antibodies elicited by Zika virus  
775 infection. *Science* **353**, aaf8505 (2016).
- 776

## 777 **FIGURE LEGENDS**

778 **Figure 1.** VIR-7831 and VIR-7831 bind S and neutralize SARS-CoV-2 virus and S variants of concern in  
779 vitro. a) Binding of VIR-7831 (black circles) and VIR-7832 (blue squares) to SARS-CoV-2 RBD was  
780 tested by ELISA. Shown is the average of four replicates and SD derived from three independent  
781 experiments. b) Association and dissociation profiles of VIR-7831 to SARS-CoV-2-RBD were measured  
782 using SPR. The double reference subtracted curves (shown for single replicates) are plotted together with  
783 the curve fit in black (obscured by close overlay with the data). Values are from two independent



784 experiments. c) Binding of VIR-7831 (black circles) and VIR-7832 (blue squares) to cell-surface S  
785 protein was determined by flow cytometry. Data are expressed as the percentage of the positive cells.  
786 Results shown are from one experiment and representative of three independent experiments performed.  
787 d) In vitro neutralization of live SARS-CoV-2 by different concentrations of VIR-7831 (left) and VIR-  
788 7832 (right) measured by nucleocapsid staining 6-hours post-infection. Results shown are from one  
789 experiment and representative of at least two independent experiments performed.

790 **Figure 2.** VIR-7831 (sotrovimab) retains activity in vitro against the Omicron variant in a pseudotyped  
791 virus assay. (a) Average fold change in VIR-7831 IC<sub>50</sub> compared to relative wild-type controls for S  
792 variants tested in a VSV/VeroE6 pseudotyped virus system. Data shown are averages of at least two  
793 independent experiments. (b) Representative neutralization curves from VIR-7831 tested against wild-  
794 type (WT) and Omicron pseudotyped virus in vitro.

795 **Figure 3.** VIR-7831 and VIR-7832 demonstrate effector function in vitro. In vitro effector function (a-e)  
796 activation profiles of human FcγRIIa (a), FcγRIIb (b), FcγRIIIa low-affinity (F158) (c) or FcγRIIIa high-  
797 affinity binding allele (V158) (d) using bioreporter assays using S-expressing CHO cells as the target  
798 antigen. Data points show means± SD of duplicates. NK-cell mediated killing (ADCC) of S-expressing  
799 CHO cells using freshly isolated cells from two donors previously genotyped for homozygous expression  
800 of low-affinity (F/F158) (e) or high-affinity (V/V158) FcγRIIIa (f). Data points are means of  
801 quadruplicates ± SD. g) Antibody-dependent cellular phagocytosis (ADCP) using S-expressing CHO cells  
802 and freshly isolated PBMCs. Data represent the means of duplicates ± SD.

803 **Figure 4.** VIR-7831 shows in vivo efficacy in a hamster SARS-CoV-2 model of infection. a) Overview  
804 of hamster in vivo study design. b) and c) Animal weight over time as a percent of starting weight in  
805 animals dosed a Day -1 (b) or Day -2 (c). Medians of at least N=6 animals and interquartile range are  
806 shown. d) and e) Day 4 terminal weights expressed as a percentage of starting weight for animals dosed at  
807 Day -1 (d) or Day -2 (e). Bar denotes median values. f) and g) Day 4 lung viral load in Day -1 (f) or Day -  
808 2 (g) treated animals as assessed by RT-qPCR. Bar denotes median values. h) and i) infectious virus in



809 lung at Day 4 for Day -1 (h) or Day -2 (i) dosed animals. Bar denotes median values. ns=not significant,  
810 \*\* =  $p < 0.05$ , and \*\*\* =  $< 0.005$  as assessed by the Mann-Whitney U-test.

811 **Table 1.** VIR-7831 and VIR-7832 retain activity against S variants of concern in an authentic virus  
812 system. Average fold change in VIR-7831 and VIR-7832  $IC_{50}$  compared to relative wild-type controls for  
813 S variants tested in an authentic virus system. Data shown are averages of at least two independent  
814 experiments.

815 **Table 2.** VIR-7831 and VIR-7832 retain activity against S variants of concern in a pseudotyped virus  
816 system. Average fold change in VIR-7831 and VIR-7832  $IC_{50}$  compared to relative wild-type controls for  
817 S variants tested in a VSV/VeroE6 pseudotyped virus system. Data shown are averages of at least two  
818 independent experiments.

819 **Table 3.** VIR-7831 and VIR-7832 retain activity against variants that confer resistance to authorized or  
820 approved mAbs. Activity of VIR-7831 against variants conferring reduced susceptibility to  
821 bamlanivimab, imdevimab or casirivimab in a VSV/VeroE6 pseudotyped virus system. The geometric  
822 mean of  $IC_{50}$ s and average fold-change versus the relative wild-type control from at least two independent  
823 experiments are shown.

824 **Table 4.** The VIR-7831/VIR-7832 epitope is highly conserved. Conservation data comprising >4,500,000  
825 sequences from the GISAID database and variants at each position are shown. Substitutions in green were  
826 tested in a pseudotyped virus assay.

827

828 **Supplemental Figure 1.** Binding of VIR-7831 and VIR-7832 to human  $Fc\gamma$ Rs and C1q as measured by  
829 SPR. Binding of VIR-7831 and VIR-7832 to a) human  $Fc\gamma$ RIIa (H131 and R131 alleles),  $Fc\gamma$ RIIIa (F158  
830 and V158 alleles) and  $Fc\gamma$ RIIb were measured using SPR. Biotinylated purified  $Fc\gamma$ Rs were captured on  
831 the sensor chip surface prior to injection of VIR-7831 or VIR-7832. Association and dissociation profiles  
832 (separated by the vertical dotted line) were measured in real time as change in the SPR signal. b) Binding

833 of VIR-7831 and VIR-7832 to complement component C1q was measured using BLI on an Octet Red96  
834 instrument. Association and dissociation profiles (separated by the vertical dotted line) were measured in  
835 real time as change in the interference pattern.

836 **Supplemental Figure 2.** Sub-neutralizing concentrations of VIR-7831 and VIR-7832 do not enhance  
837 viral entry, viral replication or cytokine production in vitro. Internalization (a) and replication (b) of  
838 SARS-CoV-2 was evaluated in VeroE6, moDCs or PBMCs at various timepoints. Two independent  
839 experiments with human moDCs and PBMCs from three individual donors were analyzed (5 unique  
840 moDC donors, 6 unique PBMC donors total between two experiments). VeroE6 cells were run in  
841 duplicate for both independent experiments. Data from each replicate well from two independent  
842 experiments are plotted as individual points, with horizontal lines representing the median. Mann-  
843 Whitney U-test comparison to no antibody group, \* $p < 0.05$ . c) Supernatant cytokine and chemokine levels  
844 as measured by MSD at the indicated time post infection. Data from two independent experiments (three  
845 replicates each, five unique donors) are plotted as the mean and SD.

846 **Supplemental Figure 3.** Overview of VIR-7832 resistance selection method. All passaging was  
847 conducted in duplicate wells. (a) VIR-7832 concentration was increased during each passage. P3 X  
848 indicates passage 3 virus, after which virus was lost with subsequent increases in concentration. In (b) and  
849 (c), p3X denotes where passage 3 virus from (a) was used to initiate (b) viral lineage 1 and (c) viral  
850 lineage 2. Arrows indicate passages that were subjected to sequence analysis, and \* indicate the passages  
851 in lineage 1 with no detectable virus or CPE. Selection continued for a total of eight passages.

852 **Supplemental Table 1.** Amino acid substitutions identified in the SARS-CoV-2 S upon in vitro selection  
853 with VIR-7832. Spike gene sequences were compared to a SARS-CoV-2 reference sequence (NCBI:  
854 NC\_045512.2) to identify variants. Fold-changes in  $IC_{50}$  were determined compared to the SARS-CoV-2  
855 virus stock.

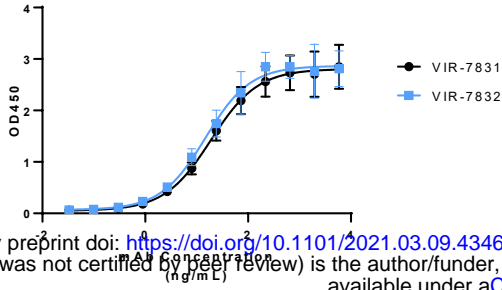
856 **Supplemental Table 2.** VIR-7831 and VIR-7832 activity against selected S variants. VIR-7831/VIR-  
857 7832 epitope variants observed by in vitro resistance selection were individually tested in a VSV/VeroE6  
858 pseudotyped virus system. The geometric mean of  $IC_{50}$ s and average fold-change versus the relative wild-  
859 type control from at least two independent experiments are shown.

860 **Supplemental Table 3.** Activity of VIR-7831 against epitope variants. VIR-7831/VIR-7832 epitope  
861 variants detected in sequences from the GISAID database were tested in a VSV/VeroE6 pseudotyped  
862 virus system. The geometric mean of  $IC_{50}$ s and average fold-change versus the relative wild-type control  
863 from at least two independent experiments are shown.

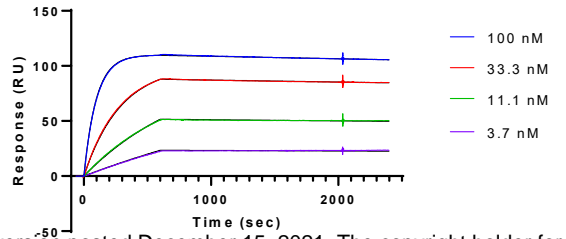
864

Figure 1

a)

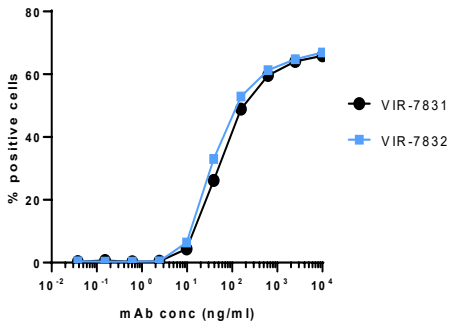


b)



bioRxiv preprint doi: <https://doi.org/10.1101/2021.03.09.434607>; this version posted December 15, 2021. The copyright holder for this preprint (which was not certified by peer review) is the author/funder, who has granted bioRxiv a license to display the preprint in perpetuity. It is made available under aCC-BY-NC-ND 4.0 International license.

c)



d)

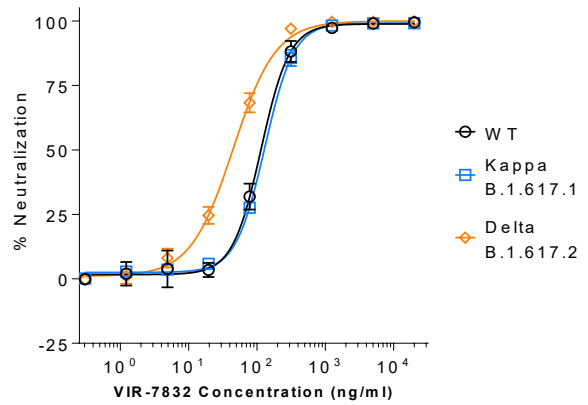
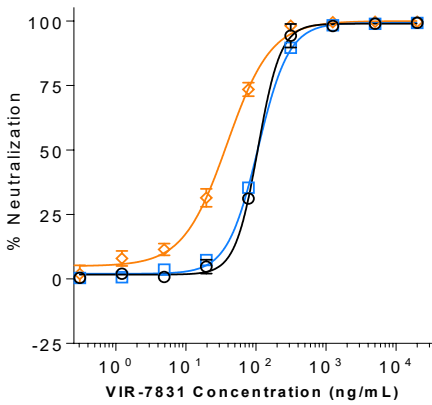
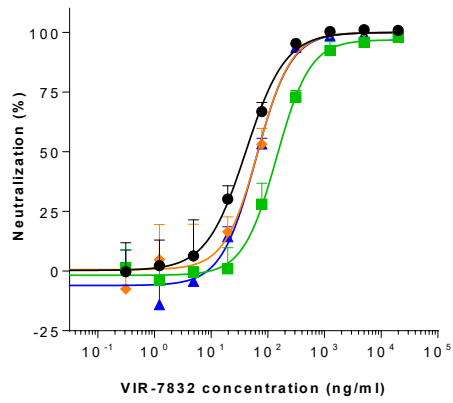
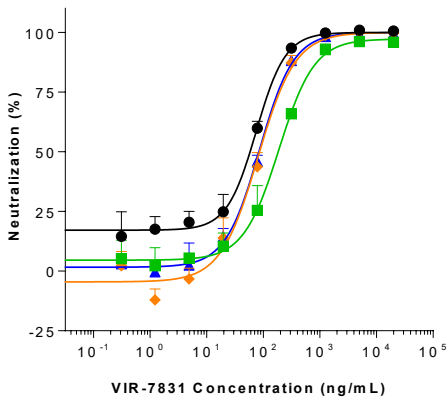


Figure 2

a)

Spike Domain	Substitution	Fold-Change in VIR-7831 IC <sub>50</sub> Compared to Wild-Type
N-Terminal Domain	del69-70	0.9 <sup>a</sup>
	T95I	0.6 <sup>b</sup>
	G142D	1.0 <sup>c</sup>
Receptor Binding Domain	G339D	1.2
	R346K	0.7
	S375F	0.5
	K417N	0.6
	G446S	1.5(V) <sup>d</sup>
	E484A	0.4
	N440K	0.5
	S477N	2.0
	T478K	0.6
	Q493R	0.9
	N501Y	0.6
S1/S2	D614G	1.0
	H655Y	0.4 <sup>e</sup>
	P681H	0.9
Combination of 37 Omicron Spike Substitutions	A67V, H69del, V70del, T95I, G142D, V143del, Y144del, Y145del, N211del, L212I, ins214EPE, G339D, S371L, S373P, S375F, K417N, N440K, G446S, S477N, T478K, E484A, Q493R, G496S, Q498R, N501Y, Y505H, T547K, D614G, H655Y, N679K, P681H, N764K, D796Y, N856K, Q954H, N969K, L981F	2.7

bioRxiv preprint doi: <https://doi.org/10.1101/2021.03.09.434607>; this version posted December 15, 2021. The copyright holder for this preprint (which was not certified by peer review) is the author/funder, who has granted bioRxiv a license to display the preprint in perpetuity. It is made available under aCC-BY-NC-ND 4.0 International license.

a Substitution tested in the context of variant B.1.258

b Substitution tested in the context of the Iota and Kappa variants

c Substitution tested in the context of the Delta and Delta Plus variants

d Data shown are for an alternative mutation (in parentheses) at the same position

e Substitution tested in the context of the Gamma variant

b)

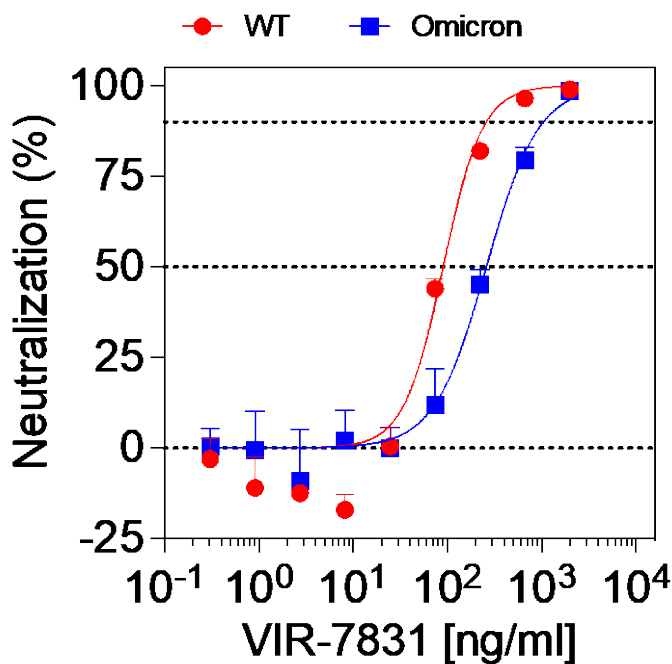


Figure 3

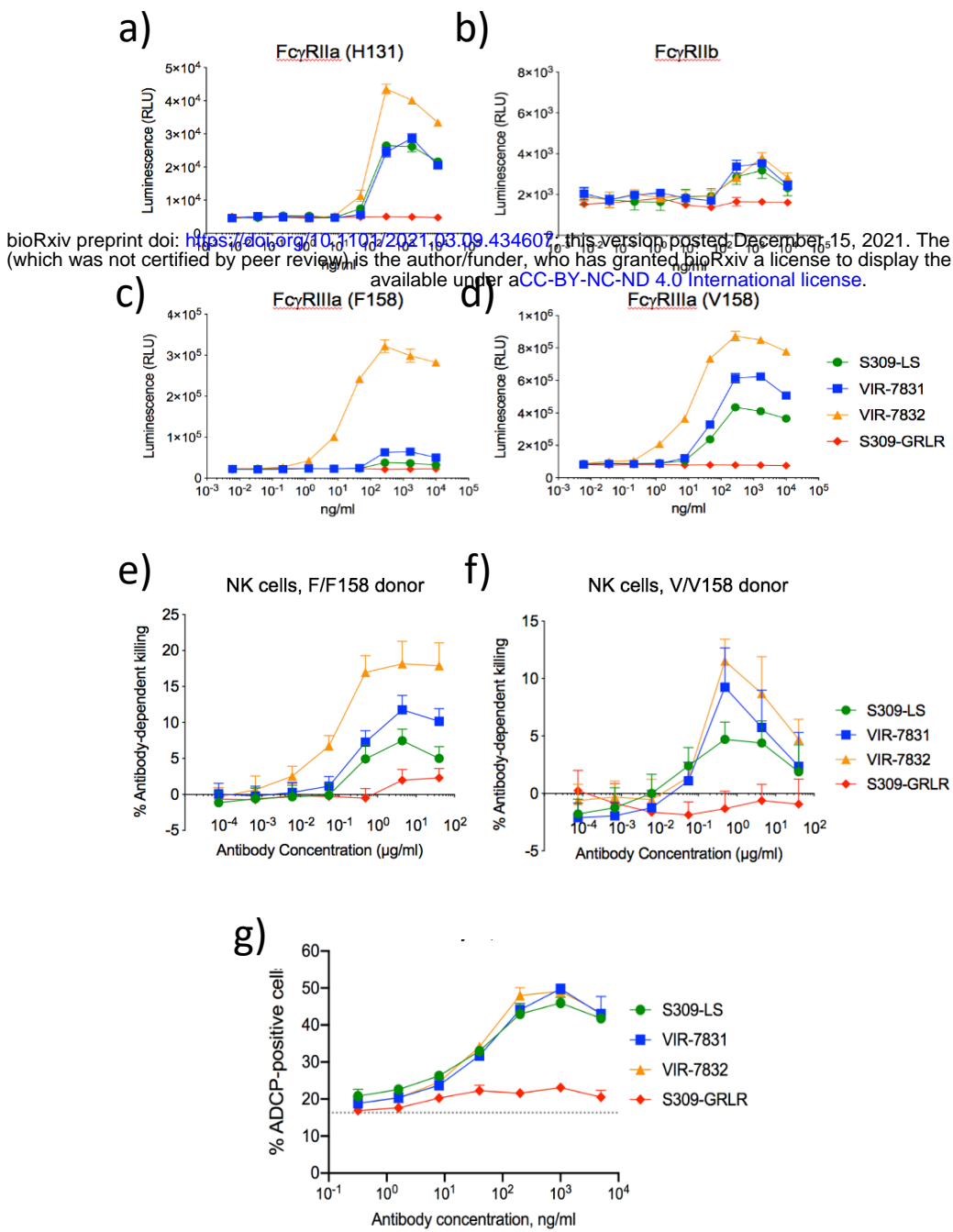


Figure 4

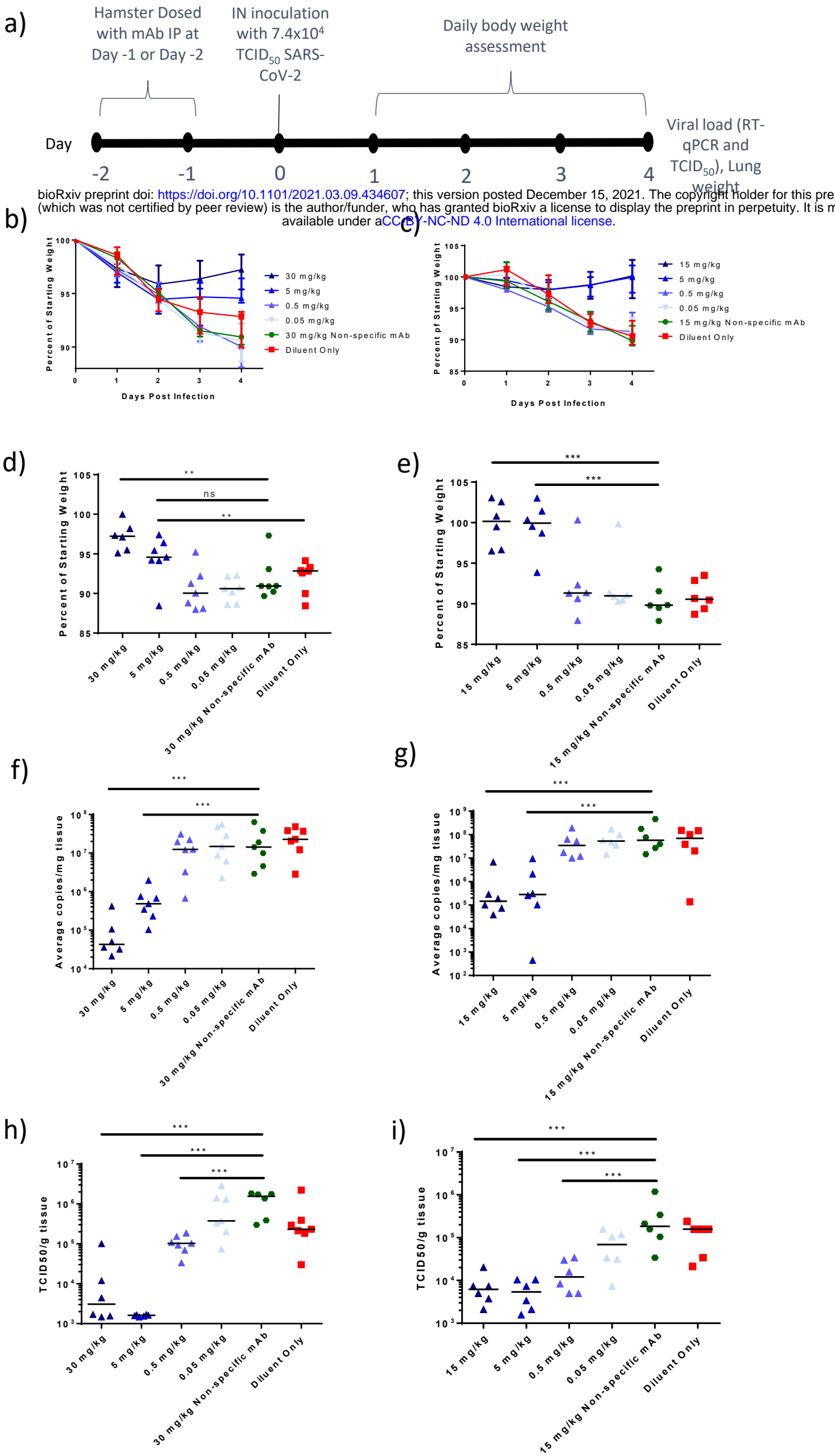


Table 1

<b>SARS-CoV-2 Variant</b>	<b>Geometric Mean VIR-7831 IC<sub>50</sub> (ng/ml) (Average Fold Change IC<sub>50</sub> vs. Wild-Type)</b>	<b>Geometric Mean VIR-7831 IC<sub>90</sub> (ng/ml) (Average Fold Change IC<sub>90</sub> vs. Wild-Type)</b>	<b>Geometric Mean VIR-7832 IC<sub>50</sub> (ng/ml) (Average Fold Change IC<sub>50</sub> vs. Wild-Type)</b>	<b>Geometric Mean VIR-7832 IC<sub>90</sub> (ng/ml) (Average Fold Change IC<sub>90</sub> vs. Wild-Type)</b>
Alpha (B.1.1.7)	187.15 (3.0)	1246.86 (4.1)	181.12 (3.1)	1222.95 (3.7)
Beta (B.1.351)	71.89 (1.2)	385.01 (1.3)	59.67 (1.1)	309.84 (0.9)
Gamma (P.1)	73.11 (1.6)	335.79 (1.4)	48.94 (1.2)	217.02 (0.9)
Delta (B.1.617.2)	51.29 (0.4)	219.08 (0.6)	59.13 (0.5)	274.24 (0.7)
Kappa (B.1.617.1)	118.64 (0.9)	379.89 (1.0)	132.37 (1.0)	428.83 (1.0)

bioRxiv preprint doi: <https://doi.org/10.1101/2021.03.09.434607>; this version posted December 15, 2021. The copyright holder for this preprint (which was not certified by peer review) is the author/funder, who has granted bioRxiv a license to display the preprint in perpetuity. It is made available under aCC-BY-NC-ND 4.0 International license.



Table 2

Variant	Spike Mutations	Fold-Change in VIR-7831 IC <sub>50</sub> vs. Wild-type	Fold-Change in VIR-7832 IC <sub>50</sub> vs. Wild-type
Alpha (B.1.1.7)	H69-, V70-, Y144-, N501Y, A570D, D614G, P681H, T716I, S982A, D1118H	2.3	2.5
Beta (B.1.351)	L18F, D80A, D215G, R246I, K417N, E484K, N501Y, D614G, A701V	0.6	0.7
Gamma (P.1)	D138Y, D614G, E484K, H655Y, K417T, L18F, N501Y, P26S, R190S, T1027I, T20N, V1176F	0.4	0.4
Delta (B.1.617.2)	T19R, G142D, E156G, F157-, R158-, L452R, T478K, D614G, P681R, D950N	1	NT
Epsilon (B.1.427/B.1.429)	S13I, W152C, L452R, D614G	0.7	NT
Eta (B.1.525)	Q52R, A67V, H69-, V70-, Y144-, E484K, D614G, Q677H, F888L	0.9	NT
Iota (B.1.526)	L5F, T95I, D253G, E484K, D614G, A701V	0.6	NT
Kappa (B.1.617.1)	T95I, G142D, E154K, L452R, E484Q, D614G, P681R, Q1071H	0.7	NT
Lambda (C.37)	G75V, T76I, del246-252, L452Q, F490S, T859N	1.5	NT
Delta Plus (AY.1)	T19R, T95I, G142D, E156G, F157-, R158-, W258L, K417N, L452R, T478K, D614G, P681R, D950N	1.1	NT
Delta Plus (AY.2)	T19R, V70F, G142D, E156G, F157-, R158-, A222V, K417N, L452R, T478K, D614G, P681R, D950N	1.3	NT
Delta Plus (AY. 4.2)	T19R, T95I, G142D, Y145H, E156G, F157, R158-, A222V, L452R, T478K, D614G, P681R, D950N	1.6	NT
Mexico/Swiss (B.1.1.519)	T478K, D614G, P681H, T732A	0.8	NT
Scotland (B.1.258)	H69-, V70-, N439K, D614G	0.9	NT
US (R.2)	E484K, D614G, Q677H, T732S, E1202Q	0.8	NT
Liverpool (A.23.1)	R102I, F157L, V367F, E484K, Q613H, P681R	1.1	NT
Cameroon (B.1.619)	I210T, N440K, E484K, D614G, D936N, S939F, T1027I	1.3	NT
Bristol (B.1.1.7+E484K)	H69-, V70-, Y144-, E484K, N501Y, A570D, D614G, P681H, T716I, S982A, D1118H	1.7	NT
Mu (B.1.621)	T95I, Y144T, Y145S, ins146N, R346K, E484K, N501Y, D614G, P681H, D950N	1.3	NT

bioRxiv preprint doi: <https://doi.org/10.1101/2021.03.09.434607>; this version posted December 15, 2021. The copyright holder for this preprint (which was not certified by peer review) is the author/funder, who has granted bioRxiv a license to display the preprint in perpetuity. It is made available under aCC-BY-NC-ND 4.0 International license.

Table 3

Amino Acid position	Substitution / Deletion	mAb with Reduced Susceptibility	Variants in Tested Spike Sequence	VIR-7831 IC <sub>50</sub> (n=3)	Average Fold Change in IC <sub>50</sub> Compared to Relative Wild-Type
E406	W	casirivimab, imdevimab		12.71	0.74
K417	E	casirivimab	K417E	67.71	0.89
N439	K	imdevimab	N439K, D614G	17.05	0.86
N440	D	imdevimab	N440D	80.47	1.29
N440	K	imdevimab	N440K, D614G	19.99	0.48
K444	Q	imdevimab	K444Q	79.68	1.11
V445	A	imdevimab	V445A	41.74	3.38
G446	V/I	imdevimab	G446V, D614G	18.41	1.50
Y453	F	casirivimab	G261D, Y453F	27.28	2.19
L455	F	casirivimab	L455F, D614G	21.65	0.56
G476	S	casirivimab	G476S	36.97	2.94
E484	K	bamlanivimab	E484K, D614G	12.91	0.33
F486	V/I	casirivimab	F486V	82.24	1.10
Y489	H	casirivimab	Y489H	92.29	1.48
F490	S	bamlanivimab	F490S	33.10	0.85
Q493	K	casirivimab, bamlanivimab	Q483K	69.79	0.98
S494	P	casirivimab, bamlanivimab	S494P, D614G	29.10	2.50

bioRxiv preprint doi: <https://doi.org/10.1101/2021.03.09.434657>; this version posted December 15, 2021. The copyright holder for this preprint (which was not certified by peer review) is the author/funder, who has granted bioRxiv a license to display the preprint in perpetuity. It is made available under aCC-BY-NC-ND 4.0 International license.

Table 4

Amino Acid Position	Reference Amino Acid <sup>a</sup>	Substitutions Identified in order of Prevalence <sup>b</sup>	Percent Reference AA Conservation
332	I	V, T, N, D, S	>99.99
333	T	K, V, S, H, D, T, E, L, I	>99.99
334	N	K, V, S, H, D, T, E, L, I	>99.99
335	L	F, V, S, -, G, M	>99.99
336	C	S*, -, P, R	>99.99
337	P	L, S, T, H, R, -, K	>99.99
339	G	D, S, C, V, F, -, N	99.98
340	E	D, K, A, G, Q, V, -, I	>99.99
341	V	I, F, A, -, G, L, P, S	>99.99
343	N	Y, -, D, K, S	>99.99
344	A	S, T, V, D, F, G, -, P	99.97
345	T	S, I, -, N	>99.99
346	R	K, S, I, G, T, -, F	99.66
354	N	K, D, S, T, H, Y, I, -, G, P	99.95
356	K	R, N, E, Q, M, T, -, G, W, Y, I, KR	99.98
357	R	K, I, -, T, G, S, C, L, RIS	99.95
358	I	V, L, F, -, T*, A, E*	>99.99
359	S	N, T, G, R, I, -, C, F	99.98
360	N	Y, S, -, K, D, F, T, A, L	>99.99
361	C	T*, -, G*, N*, F*, R*, S*, Y	>99.99
440	N	K, S, Y, T, D, I, E, -, F, H, R	99.79
441	L	R, F, I, P, V, -, Y, H, M, S, E, N	>99.99
509	R	-, K*, S*, T*, I*, H	>99.99

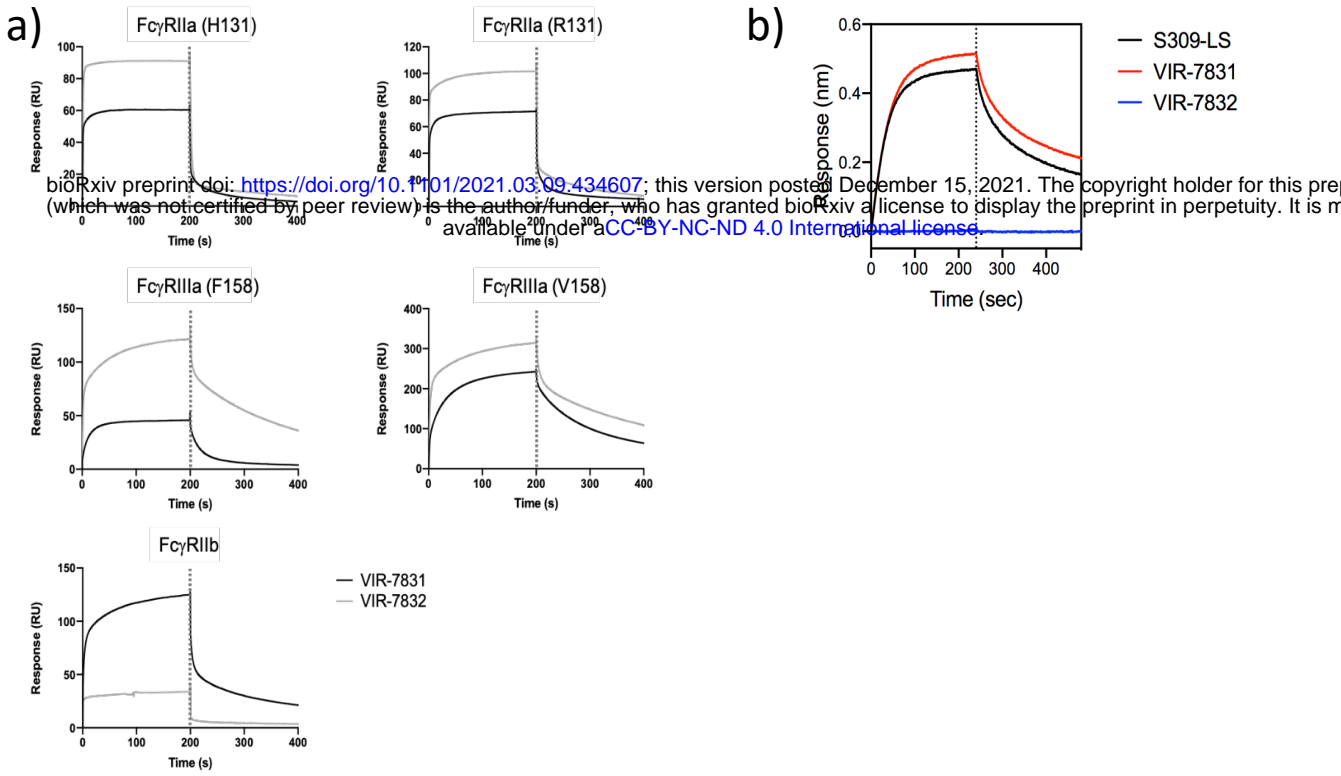
AA = amino acid

<sup>a</sup>NCBI reference sequence: YP\_009724390.1

<sup>b</sup>Dash indicates a stop codon. Asterisks indicate the substitution could not be evaluated due to low expression of the spike protein containing this substitution

bioRxiv preprint doi: <https://doi.org/10.1101/2021.03.09.434607>; this version posted December 15, 2021. The copyright holder for this preprint (which was not certified by peer review) is the author/funder, who has granted bioRxiv a license to display the preprint in perpetuity. It is made available under aCC-BY-NC-ND 4.0 International license.

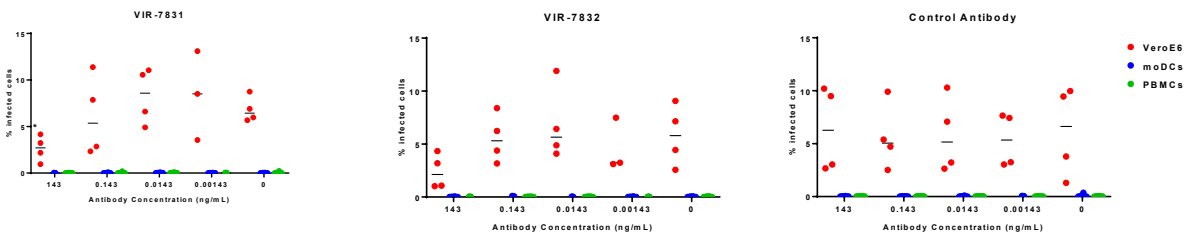
# Supplemental Figure 1



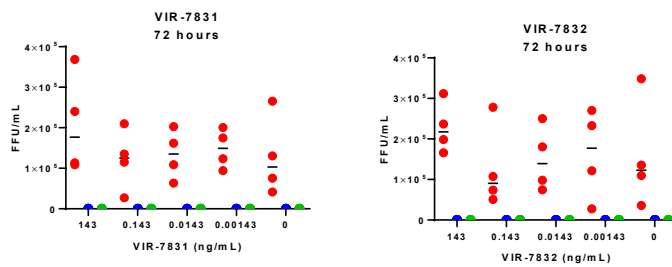
# Supplemental Figure 2

bioRxiv preprint doi: <https://doi.org/10.1101/2021.03.09.434607>; this version posted December 15, 2021. The copyright holder for this preprint (which was not certified by peer review) is the author/funder, who has granted bioRxiv a license to display the preprint in perpetuity. It is made available under aCC-BY-NC-ND 4.0 International license.

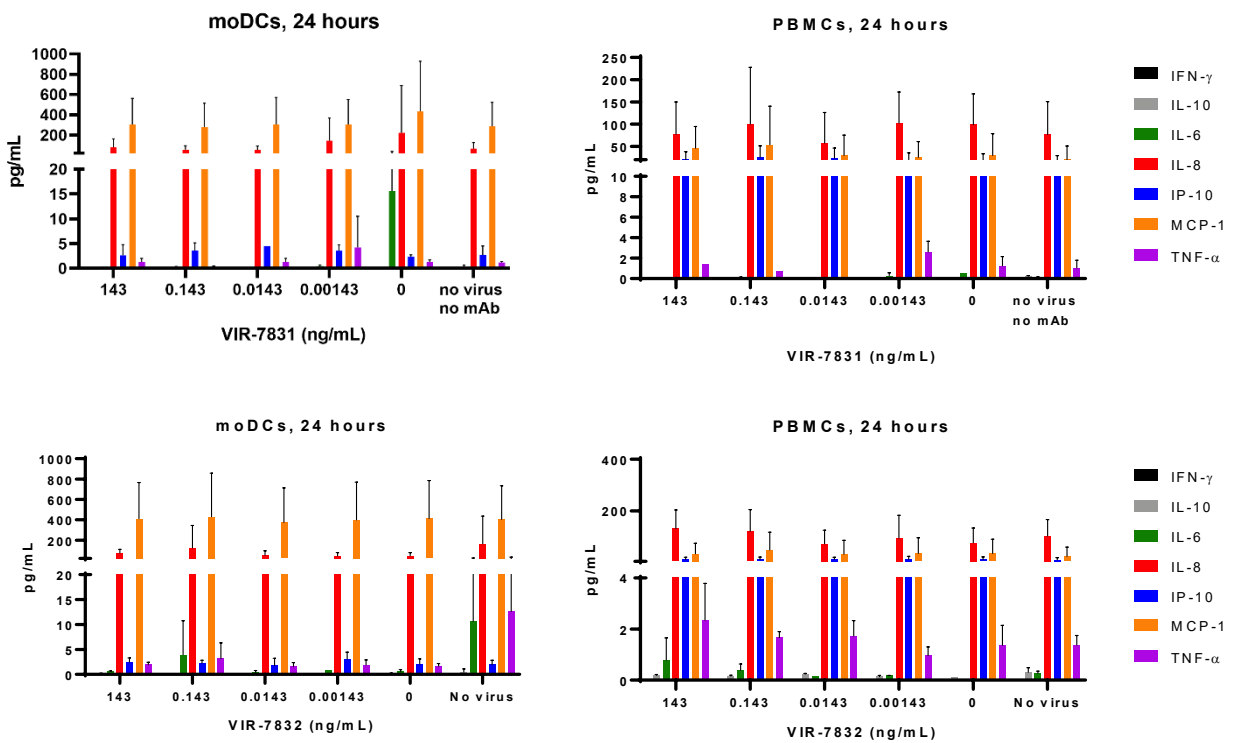
a)



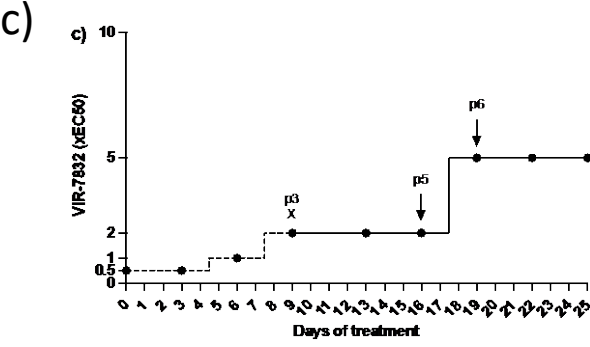
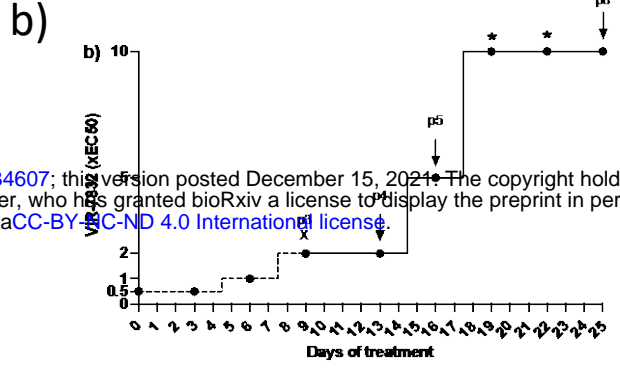
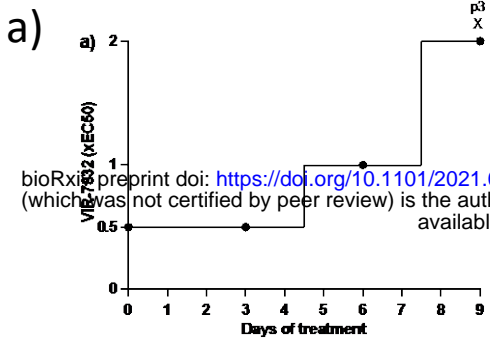
b)



c)



# Supplemental Figure 3



bioRxiv preprint doi: <https://doi.org/10.1101/2021.03.09.434607>; this version posted December 15, 2021. The copyright holder for this preprint (which was not certified by peer review) is the author/funder, who has granted bioRxiv a license to display the preprint in perpetuity. It is made available under aCC-BY-NC-ND 4.0 International license.

# Supplemental Table 1

Passage	Spike Gene Amino Acid Substitution (Freq) <sup>a,b</sup>	EC <sub>50</sub> (µg/mL)	Fold Change in EC <sub>50</sub> to WT <sup>c</sup>
SARS-CoV-2 virus stock <sup>c</sup> bioRxiv preprint doi: <a href="https://doi.org/10.1101/2021.03.09.434607">https://doi.org/10.1101/2021.03.09.434607</a> ; this version posted December 15, 2021. The copyright holder for this preprint (which was not certified by peer review) is the author/funder, who has granted bioRxiv a license to display the preprint in perpetuity. It is made available under aCC-BY-NC-ND 4.0 International license.	H66R (5.7%) S74P (10.6%) T76I (5.6%) 215-216insKLRS (60.9%) H655Y (3.1%)	0.06	NA
VIR-7832 Lineage 1, passage 4	215-216insKLRS (74.5%) 675-679 del (20.6%)	0.34	5.64
VIR-7832 Lineage 1, passage 5	215-216insKLRS (74.6%) 675-679del (66.0%)	0.35	5.93
VIR-7832 Lineage 1, passage 8	215-216insKLRS (74.7%) E340A (98.7%) 675-679del (84.5%)	ND	>10
VIR-7832 Lineage 2, passage 5	215-216insKLRS (73.9%) 675-679del (47.3%) R682W (4.9%) V1128F (3.5%)	0.32	5.40
VIR-7832 Lineage 2, passage 6	215-216insKLRS (75.3%) 675-679del (74.2%) R682W (4.9%) V1128F (30.9%)	0.39	6.54



## Supplemental Table 2

Amino Acid Changes in Spike protein	VIR-7831		VIR-7832	
	Geomean Neutralization IC <sub>50</sub> (ng/mL)	Fold Change Relative to Wild-Type	Geomean Neutralization IC <sub>50</sub> (ng/mL)	Fold Change Relative to Wild-Type
Wild Type	104.46	NA	100.75	NA
E340A	> 10,000	> 107	> 10,000	> 107
R682W	53.96	0.52	47.78	0.49
V1128F	50.65	0.53	49.69	0.60

bioRxiv preprint doi: <https://doi.org/10.1101/2021.03.09.434607>; this version posted December 15, 2021. The copyright holder for this preprint (which was not certified by peer review) is the author/funder, who has granted bioRxiv a license to display the preprint in perpetuity. It is made available under aCC-BY-NC-ND 4.0 International license.

## Supplemental Table 3

Epitope Reference Amino Acid	Amino Acid Substitutions in Spike Protein	Geomean Neutralization IC <sub>50</sub> (ng/mL)	Average Fold Change IC <sub>50</sub> Relative to Reference <sup>a</sup>
I332	I332V, D614G	59.43	1.48
I332	I332T, D614G	66.74	1.61
T333	T333K, D614G	22.14	0.67
	T333I, D614G	30.93	0.59
N334	N334K, D614G	45.36	1.27
	N334H, D614G	30.74	0.87
	N334S, D614G	34.37	1.13
	N334Y, D614G	32.89	0.96
L335	L335F	29.19	0.81
	L335S, D614G	29.8	0.85
	L335V, D614G	42.2	0.63
P337	P337H, D614G	185.29	5.13
	P337L, D614G	>10000	>192
	P337K, D614G	>10000	>304
	P337R, D614G	>10000	>192
	P337S, D614G	127.69	1.26
	P337T, D614G	383.27	10.62
G339	G339D, D614G	117.38	1.18
	G339S, D614G	32.67	0.86
	G339C, D614G	68.79	1.18
	G339V, D614G	78.32	1.26
E340	E340A	>10000	>100
	E340D, D614G	81.46	2.45
	E340K	>10000	>297
	E340G, D614G	640.07	18.21
	E340Q, D614G	>2500	>50
	E340V, D614G	>10000	>200
V341	V341I, D614G	14.6	0.16
N343	N343S, D614G	16.87	0.48

bioRxiv preprint doi: <https://doi.org/10.1101/2021.09.09.434607>; this version posted September 15, 2021. The copyright holder for this preprint (which was not certified by peer review) is the author/funder, who has granted bioRxiv a license to display the preprint in perpetuity. It is made available under aCC-BY-NC-ND 4.0 International license.

## Supplemental Table 3 (con't)

Epitope Reference Amino Acid	Amino Acid Substitutions in Spike Protein	Geomean Neutralization IC <sub>50</sub> (ng/mL)	Average Fold Change IC <sub>50</sub> Relative to Reference <sup>a</sup>
A344	A344S	92.19	0.89
	A344V, D614G	53.87	1.14
	A344D, D614G	131.53	2.57
T345	T345S, D614G	42.92	0.69
	T345N, D614G	20.29	0.57
	T345I, D614G	11.78	0.20
R346	R346I, D614G	65.39	1.72
	R346S, D614G	42.87	1.13
	R346T, D614G	89.04	1.25
	R346K, D614G	24.76	0.72
	R346G, D614G	43.73	0.85
N354	N354D	104.8	1.00
	N354K, T95I	70.62	0.76
	N354H, D614G	74.88	1.06
	N354K, T95I	70.62	0.76
	N354S, D614G	61.78	0.89
	N354I, D614G	37.09	1.05
	N354T, D614G	43.32	0.65
	N354Y, D614G	67.63	1.08
K356	K356A	111.18	1.06
	K356R, D614G	29.61	0.78
	K356N, D614G	53.22	1.12
	K356M, D614G	64.09	1.03
	K356T, D614G	281.13	5.9
	K356E, D614G	76.54	1.65
	K356Q, D614G	43.2	0.94
R357	R357K, D614G	39.13	1.02
	R357I, D614G	46.41	0.98

bioRxiv preprint doi: <https://doi.org/10.1101/2021.03.09.434607>; this version posted December 15, 2021. The copyright holder for this preprint (which was not certified by peer review) is the author/funder, who has granted bioRxiv a license to display the preprint in perpetuity. It is made available under aCC-BY-NC-ND 4.0 International license.

## Supplemental Table 3 (con't)

Epitope Reference Amino Acid	Amino Acid Substitutions in Spike Protein	Geomean Neutralization IC <sub>50</sub> (ng/mL)	Average Fold Change IC <sub>50</sub> Relative to Reference <sup>a</sup>
I358	I358V, D614G	44.01	0.8
	I358F, D614G	42.69	1.19
S359	S359N	95.55	0.96
	S359G, D614G	37.56	0.8
	S359R, D614G	62	0.89
	S359T, D614G	39.98	0.84
	S359I, D614G	38.01	0.84
N360	N360S, D614G	34.08	0.72
	N360Y, D614G	29.67	0.61
N440	N440D	80.47	1.29
	N440Y, D614G	42.65	0.68
	N440S, D614G	51.34	0.73
	N440K, D614G	19.99	0.48
	N440I, D614G	40.21	1.22
	N440T, D614G	50.81	0.82
	N440E, D614G	46.97	0.80
	N440F, D614G	43.07	0.85
L441	L441F, D614G	25.21	0.4
	L441I, D614G	32.96	0.7
	L441R, D614G	42.3	0.87
	L441V, D614G	48.24	0.98
	L441P, D614G	44.95	0.76

bioRxiv preprint doi: <https://doi.org/10.1101/2021.12.15.4607>; this version posted December 15, 2021. The copyright holder for this preprint (which was not certified by peer review) is the author/funder, who has granted bioRxiv a license to display the preprint in perpetuity. It is made available under aCC-BY-NC-ND 4.0 International license.